

Role of pathogen-laden expiratory droplet dispersion and natural ventilation explaining a COVID-19 outbreak in a coach bus

Article

Accepted Version

Creative Commons: Attribution-Noncommercial-No Derivative Works 4.0

Luo, Q., Ou, C., Hang, J., Luo, Z. ORCID: <https://orcid.org/0000-0002-2082-3958>, Yang, H., Yang, X., Zhang, X., Li, Y. and Fan, X. (2022) Role of pathogen-laden expiratory droplet dispersion and natural ventilation explaining a COVID-19 outbreak in a coach bus. *Building and Environment*, 220. 109160. ISSN 0360-1323 doi: <https://doi.org/10.1016/j.buildenv.2022.109160> Available at <https://centaur.reading.ac.uk/104958/>

It is advisable to refer to the publisher's version if you intend to cite from the work. See [Guidance on citing](#).

To link to this article DOI: <http://dx.doi.org/10.1016/j.buildenv.2022.109160>

Publisher: Elsevier

All outputs in CentAUR are protected by Intellectual Property Rights law, including copyright law. Copyright and IPR is retained by the creators or other copyright holders. Terms and conditions for use of this material are defined in the [End User Agreement](#).

www.reading.ac.uk/centaur

CentAUR

Central Archive at the University of Reading

Reading's research outputs online

1 To be submitted to Building and Environment 2022

2

3 **Role of pathogen-laden expiratory droplet dispersion and natural ventilation**
4 **explaining a COVID-19 outbreak in a coach bus**

5

6 Qiqi Luo^{a,b,#}, Cuiyun Ou^{a,b,#}, Jian Hang^{a,b*}, Zhiwen Luo^c, Hongyu Yang^{a,b}, Xia

7 Yang^{a,b}, Xuelin Zhang^{a,b}, Yuguo Li^d, Xiaodan Fan^{a,b}

8

9 ^a School of Atmospheric Sciences, Sun Yat-sen University, and Southern Marine
10 Science and Engineering Guangdong Laboratory (Zhuhai), Zhuhai, China

11 ^b Key Laboratory of Tropical Atmosphere-Ocean System (Sun Yat-sen University),
12 Ministry of Education, Zhuhai (519000), China

13 ^c School of the Built Environment, University of Reading, Reading, UK

14 ^d Department of Mechanical Engineering, The University of Hong Kong, Hong Kong
15 SAR, China

16

17 # First authors: Qiqi Luo, Cuiyun Ou

18

19 *Corresponding author: Jian Hang

20 School of Atmospheric Sciences, Sun Yat-sen University, Zhuhai, China

21 Tel: +86-13710248541

22 E-mail address: hangj3@mail.sysu.edu.cn

23

24

Abbreviations			
<i>ACH</i>	Air change rates per hour [h^{-1}]	<i>N</i>	Total released droplet number
ASHRAE	American Society of Heating, Refrigerating and Air-Conditioning Engineers	<i>n</i>	Number of droplets
<i>C</i>	Particle concentration [$\mu\text{g}/\text{m}^3$]	NMSE	Normalized mean square error
C_2H_6	Ethane	N_i	Passenger inhaled droplet number
C_c	Cunningham slip correction	N_s	Passenger inhaled pathogen-laden droplet number
CCTV	Closed-circuit television	<i>p</i>	Pulmonary ventilation rate [m^3/s]
C_d	Quantum concentration of droplets [quanta/ m^3]	<i>P</i>	Infection risk
C_e	Particle concentration at exhaust [$\mu\text{g}/\text{m}^3$]	PLD	Pathogen-laden droplets
CFD	Computational fluid dynamics	p_s	Pulmonary ventilation rate of index patient [m^3/s]
C_g	Tracer gas concentration	<i>q</i>	Quanta generation rate [quanta/s]
$C_{g,p}$	Tracer gas concentration at passenger's nose [ppm]	<i>Q</i>	Ventilation rate [m^3/s]
$C_{g,q}$	Quantum concentration of tracer gas [quanta/ m^3]	Re_p	Reynolds number
$C_{g,s}$	Tracer gas concentration at patient [ppm]	<i>RH</i>	Ambient relative humidity
$C_{i,s}$	Vapor concentration at droplet surface [$\text{kg}\cdot\text{mol}\cdot\text{m}^{-3}$]	RNG	Renormalization group
$C_{i,sr}$	Vapor concentration of bulk [$\text{kg}\cdot\text{mol}\cdot\text{m}^{-3}$]	SARS-CoV-2	Severe acute respiratory syndrome coronavirus 2
$C_{infected}$	Number of infected cases	$S_{susceptible}$	Number of susceptible people
COVID-19	Corona virus disease 2019	<i>t</i>	Time [s]
C_s	Particle concentration at inlet [$\mu\text{g}/\text{m}^3$]	<i>T</i>	Temperature [K]
C_v	Virus concentration	t_0	Exposure period [s]
<i>D</i>	Dilution ratio	T_e	Temperature at exhaust [K]
d_p	Initial droplet diameter [μm]	<i>TIF</i>	30-minute-exposure intake fraction
$F_{a,i}$	Additional forces [N]	<i>TIR</i>	30-minute-exposure infection risk
FB	Fractional bias	T_s	Temperature at inlet [K]
f_D	Stoke's drag modification	<i>U</i>	Normalized velocity
$F_{drag,i}$	Drag force [N]	$u_{p,i}$	Droplet velocity (m/s)
$F_{g,i}$	Gravitational force [N]	u_s	Supply air velocity [m/s]
<i>g</i>	Gravitational acceleration	<i>V</i>	Velocity [m/s]
<i>H</i>	Height [m]	V_{Bus}	Speed of bus [m/s]
HVAC	Heating, Ventilation and Air Conditioning	<i>Vol</i>	Volume [m^3]
<i>I</i>	Number of infectors	<i>W</i>	Width [m]
k_c	Mass transfer coefficient [m/s]	WHO	World Health Organization
<i>L</i>	Length [m]	<i>WIR</i>	Whole-journal-exposure infection
		$x_{p,i}$	Droplet displacement [m]
		<i>Z</i>	Poles height [m]
		μ_t	Turbulent viscosity [$\text{kg}\cdot\text{m}^{-1}\cdot\text{s}^{-1}$]
		ε	Normalized particle concentration
		θ	Normalized temperature
		λ	Molecular mean free path of air [m]
		ρ	Density of air [kg/m^3]
		ρ_p	Density of droplets [kg/m^3]
		τ_p	Aerosol characteristic response

26 **Abstract**

27 The influencing mechanism of droplet transmissions inside crowded and poorly
28 ventilated buses on infection risks of respiratory diseases is still unclear. Based on
29 experiments of one-infecting-seven COVID-19 outbreak with an index patient at bus
30 rear, we conducted CFD simulations to investigate integrated effects of initial droplet
31 diameters(tracer gas, 5 μm , 50 μm and 100 μm), natural air change rates per
32 hour($ACH=0.62, 2.27$ and 5.66h^{-1} related to bus speeds) and relative humidity($RH=35\%$
33 and 95%) on pathogen-laden droplet dispersion and infection risks. Outdoor pressure
34 difference around bus surfaces introduces natural ventilation airflow entering from bus-
35 rear skylight and leaving from the front one. When $ACH=0.62\text{h}^{-1}$ (idling state), the 30-
36 minute-exposure infection risk(TIR) of tracer gas is 15.3% (bus rear) - 11.1% (bus front),
37 and decreases to 3.1% (bus rear)- 1.3% (bus front) under $ACH=5.66\text{h}^{-1}$ (high bus
38 speed).The TIR of large droplets(i.e., 100 $\mu\text{m}/50\mu\text{m}$) is almost independent of ACH ,
39 with a peak value($\sim 3.1\%$) near the index patient, because over $99.5\%/97.0\%$ of droplets
40 deposit locally due to gravity. Moreover, 5 μm droplets can disperse further with the
41 increasing ventilation. However, TIR for 5 μm droplets at $ACH=5.66\text{h}^{-1}$ stays relatively
42 small for rear passengers(maximum 0.4%), and is even smaller in the bus middle and
43 front($<0.1\%$). This study verifies that differing from general rooms, most 5 μm droplets
44 deposit on the route through the long-and-narrow bus space with large-area
45 surfaces($L\sim 11.4\text{m}$). Therefore, tracer gas can only simulate fine droplet with little
46 deposition but cannot replace 5-100 μm droplet dispersion in coach buses.

47 **Keywords:** Computational fluid dynamics (CFD) simulation, droplet dispersion,
48 infection risk (IR), natural air change rate (ACH), aerosol inhalation transmission,
49 COVID-19

50 1. Introduction

51 Respiratory infectious diseases, such as influenza, severe acute respiratory
52 syndrome (SARS) and coronavirus disease 2019 (COVID-19), have threatened public
53 health in the last two decades [1]. In particular, the recent COVID-19 pandemic is
54 caused by severe acute respiratory syndrome coronavirus 2 (SARS-CoV-2). By 27
55 January 2022, more than 352 million people had been diagnosed with COVID-19, of
56 whom more than 3.5 million had died[2]. Most of the human-to-human infections may
57 occur in various indoor environments via droplet transmissions.

58 Numerous studies have demonstrated that respiratory infections may occur
59 through the transmission of virus-laden droplets or droplet nuclei [3-5]. Pathogen-laden
60 droplets (PLD) exhaled from the infected people may be the medium of human-to-
61 human infection, because the pathogens can survive in the air for a period of time.
62 Taking the current prevalence of COVID-19 for instance, the half-life of SARS-CoV-2
63 virus in the air is reported to be on the order of magnitude of one hour [6]. Recent
64 studies have redefined that there are three main transmission routes of respiratory
65 infection: surface touch transmission, drop spray transmission and aerosol inhalation
66 transmission [7, 8]. Among them, aerosol inhalation transmission happens when air-
67 suspended PLD are inhaled by a susceptible person. Ventilation modes and hourly air
68 change rates (*ACH*) have been verified as the key factors affecting aerosol inhalation
69 transmission and indoor infection risks [9-11].

70 There have been numerous studies on indoor ventilation, droplet/tracer gas
71 dispersion and exposure analysis in inter-unit residential buildings [12-16], general
72 indoor environments with mixing or displacement ventilation [17-19], and specific
73 indoor space, for instance, restaurants [10, 20] and hospital wards [21, 22]. Particularly,

74 for the indoor environment of public transportation, most previous researches focused
75 on airplane cabins [23-25] and high-speed trains [26, 27].

76 Although the coach bus is one of the most popular transportation modes for inter-
77 city and suburban transportation, investigations on their indoor environments and
78 infection risk are limited so far [28, 29]. Due to the unopenable windows, the crowded
79 coach bus often obtains fresh air from the skylight suppliers which is related to the
80 running conditions. When the HVAC (Heating, Ventilation and Air Conditioning) is on,
81 there is only indoor circulation, resulting in an insufficiently ventilated indoor
82 environment. Therefore, the coach bus is conducive to the transmission of respiratory
83 infectious diseases, which is worthy of study.

84 Our previous researches [11] reported that there was a COVID-19 outbreak with 7
85 non-associated infected passengers on a coach bus with insufficient natural ventilation
86 in January 2020 (winter) in Hunan Province, China. In this study, we first conducted
87 field experiments, and then numerically simulated the tracer gas dispersion under the
88 measured mean ventilation condition [11]. However, since the coach bus was driving
89 in three states (high bus speed, low bus speed and idling), corresponding to different
90 natural ventilation rates, a further detailed case study is required to investigate the
91 influence of different natural ventilation rates on droplet dispersion and resulting
92 infection risk. In addition, the initial diameter of exhaled droplets is in a large range
93 (0.1-100 μm) [30, 31]. Moreover, numerous studies [18, 32, 33] have indicated that the
94 droplet evaporation correlated to initial droplet diameters and RH significantly
95 influence their gravity force and deposition effects, which integrates with turbulent
96 diffusion, drag force, Saffman's lift force, and so on. Such complicated processes

97 should be considered for more comprehensive investigations on transmission
98 mechanisms and assessments of human-to-human exposure and infection risk.

99 Many studies have confirmed that the transport behavior of droplets smaller than
100 $5\ \mu\text{m}$ is similar to that of tracer gas in a room [34-37]. However, the indoor environment
101 of the bus is different from that of ordinary rooms, because the bus is long and narrow
102 with more obstacles and more complex indoor airflow. In addition, *RH* is considered to
103 influence droplet dispersion in indoor environments[17, 32, 38]. Therefore, two
104 questions need to be answered: does tracer gas still have a similar transmission with
105 droplets smaller than $5\ \mu\text{m}$ in the bus environment? does *RH* still obviously affect
106 droplet dispersion in the buses? For the bus environments, the feasibility of adopting
107 tracer gas to replace fine droplets and the effect of *RH* on droplet dispersion need further
108 exploration.

109 In the present study, by performing computational fluid dynamics (CFD)
110 simulations, we further investigate the integrated impacts of *RH* (35%, 95%), initial
111 droplet diameters (tracer gas, $5\ \mu\text{m}$, $50\ \mu\text{m}$, $100\ \mu\text{m}$), natural ventilation rates (*ACH* =
112 $0.62\ \text{h}^{-1}$, $2.27\ \text{h}^{-1}$, $5.66\ \text{h}^{-1}$ respectively related to idling, low bus speed, and high bus
113 speed), and body thermal plumes on the evaporation and dispersion of exhaled droplets
114 in this enclosed coach bus. We also predict the difference of exposure/infection risk for
115 various pathogen-laden expiratory droplets under different conditions.

116

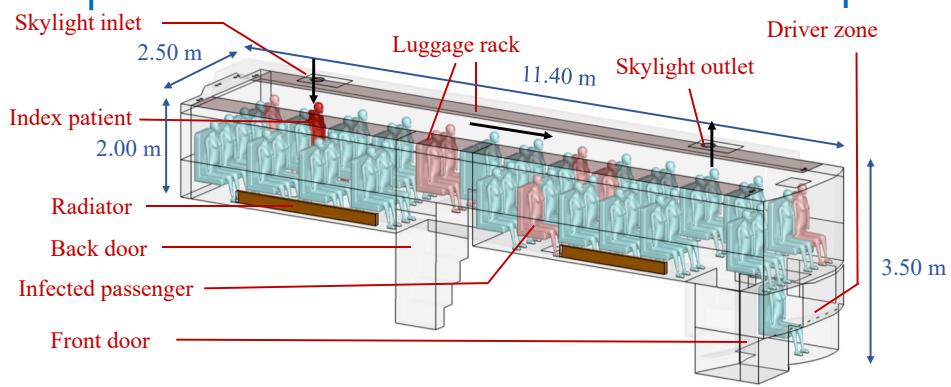
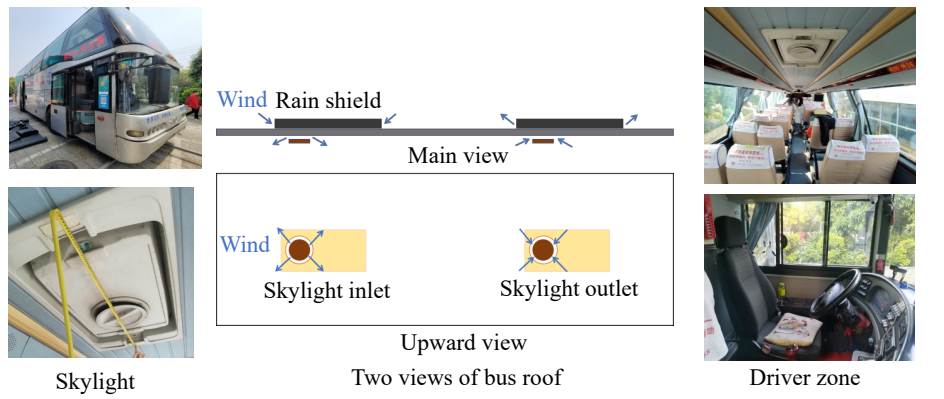
117 **2. Methodology**

118 **2.1. Full-scale experimental bus**

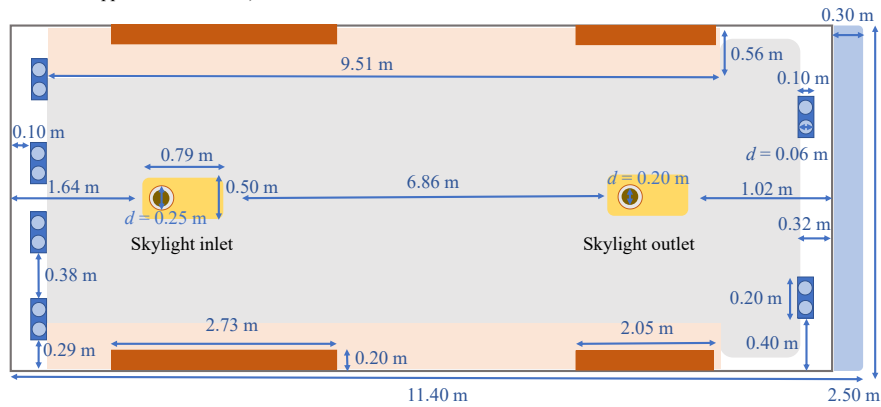
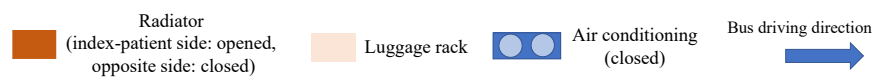
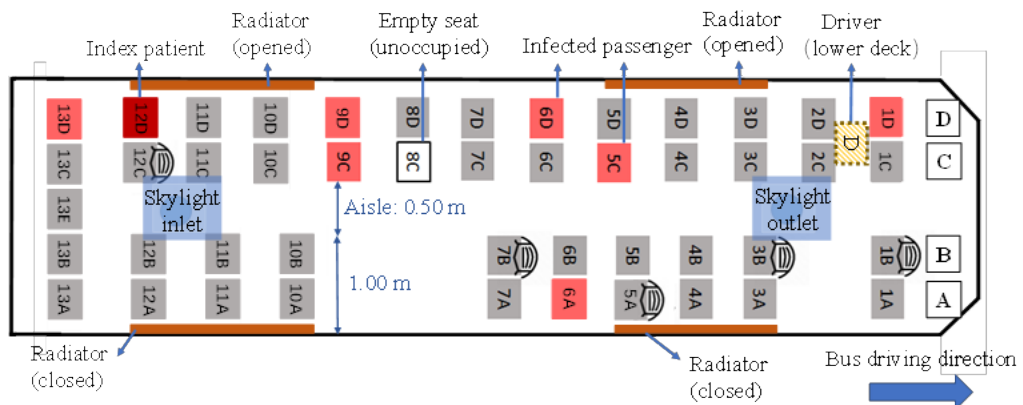
119 [Fig. 1](#) shows the detailed model descriptions of the target coach bus with a cabin
120 size of 11.4 m × 2.5 m × 2 m ($L \times W \times H$), where occurred a COVID-19 epidemic
121 during the 200-minute long-route journey on January 22, 2020 [\[11\]](#). It was a double-
122 deck 47-seat bus with the passenger cabin on the upper deck and the driver zone on the
123 lower deck. Only the radiator at the index-patient side was functional and turned on
124 during the whole journey, the other side was broken. As shown in [Fig. 1b](#), the cabin was
125 fully occupied except Seat 8C (46 passengers in total). An index patient (in scarlet) at
126 seat 12D returned home from Changsha city, Hunan province, China, eventually
127 infecting seven of the passengers. These infected passengers (in pink) were respectively
128 located at seats 1D, 5C, 6A, 6D, 9C, 9D and 13D. Among them, the passenger at seat
129 1D is farthest away from the index patient, at a distance of 9.46 m.

130 All the windows could not be opened with the skylights (as shown in [Fig. 1a](#)) for
131 natural ventilation. Fresh air entered the bus through the skylight inlet at the rear ceiling,
132 and contaminated air escaped from the skylight outlet at the front ceiling ([Fig. 1a](#)). The
133 measured ACH could change with the various air pressure difference between the
134 indoor and outdoor of the bus due to the various running speeds. More detailed
135 information about the experimental setup can be found in our previous study [\[11\]](#).

136



(a)



(b)

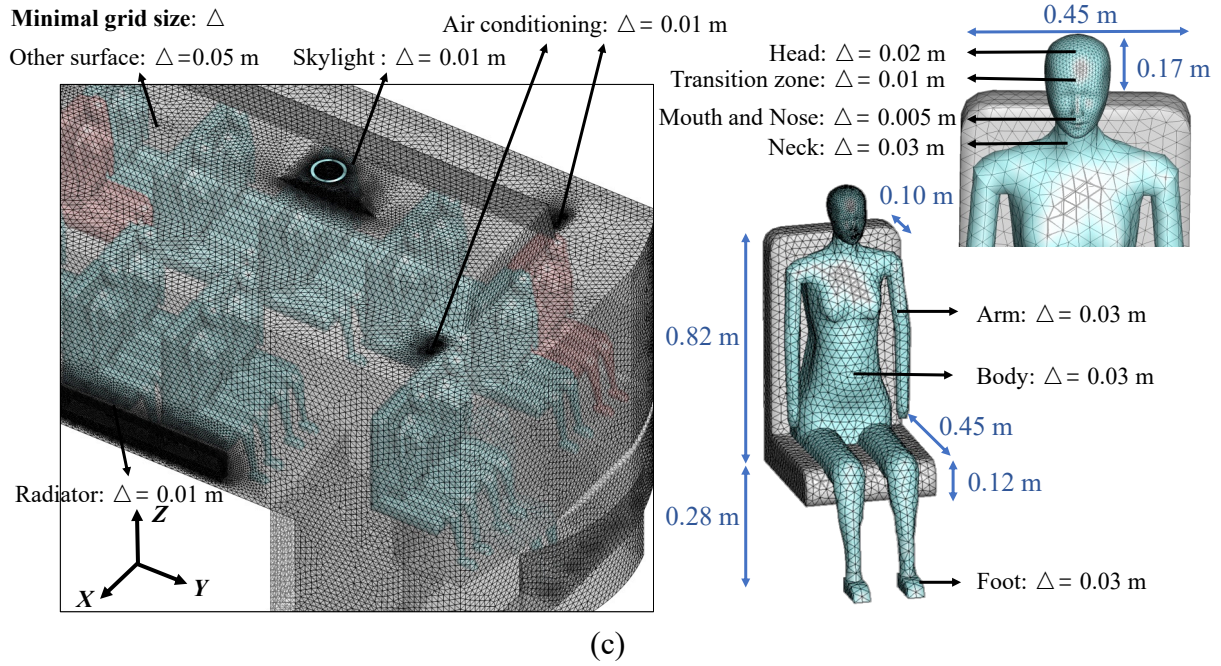


Fig. 1. (a) Bus photos and 3D bus model, (b) Bus top view and size information, (c) Grid arrangements of model.

137

138 **2.2. Numerical modeling of bus ventilation and droplet dispersion**

139 **2.2.1. Descriptions of bus model and case studies**

140 We utilized Gambit to build the bus cabin and manikin models (Fig. 1). We created
 141 a refined grid with 0.005 m size on mouth and nose, which is smaller than the grid of
 142 0.03 m size around the human body, 0.01 m mesh size on the skylight inlet/outlet and
 143 heat radiator, and 0.05 m for the bus body (Fig. 1c). A total number of 5,379,993
 144 unstructured meshes were generated, which was verified to ensure grid-independent
 145 requirements.

146 Twenty-one cases were considered as shown in Table 1. We investigated the
 147 influence of ACH (0.62, 2.27 and 5.66 h^{-1}) related to bus speed (0, 30 and 80-90 km/h),
 148 initial droplet diameters (tracer gas, $d_p = 5, 50$ and $100 \mu m$), and ambient relative
 149 humidity ($RH = 35\%, 95\%$) on the transmission of the index patient's exhaled droplets

150 and the exposure/infection risk of other passengers. Ethane (C_2H_6) was adopted as the
 151 tracer gas to explore the dispersion difference between droplets and tracer gas in the
 152 coach bus.

153

Table 1

Parameters and setups in all 21 test cases.

Experimental variables	Setup	Notes
Ventilation rate (ACH / h^{-1})	0.62 h^{-1}	Bus is at idling ($V_{Bus} = 0$ km/h).
	2.27 h^{-1}	Bus is running at low speed ($V_{Bus} = 30$ km/h).
	5.66 h^{-1}	Bus is running at high speed ($V_{Bus} = 80-90$ km/h).
Initial droplet diameter ($d_p / \mu m$)	Tracer gas	As a surrogate for fine droplets and droplet nuclei.
	5 μm	For effect of initial diameter on droplet dispersion.
	50 μm	
	100 μm	
Ambient relative humidity ($RH / \%$)	35%	For effect of RH on droplet dispersion.
	95%	

154

155 **2.2.2. Numerical simulation of airflow model**

156 The renormalization group (RNG) $k-\epsilon$ model [39] has been verified to effectively
 157 simulate indoor airflows and tracer gas dispersion with considerable accuracy and
 158 computing efficiency [40-42]. Thus, we adopted Ansys FLUENT with RNG $k-\epsilon$ model
 159 to solve the conservation equations for mass, momentum, energy, humidity and
 160 turbulence variables. All the governing equations were discretized by the finite volume
 161 method in the second-order upwind scheme. SIMPLE scheme was selected to couple
 162 the pressure and velocity. Boussinesq hypothesis was adopted to consider the influence
 163 of thermal buoyancy.

164 To simulate the airflow field, we assumed that the variables were unchanging
 165 (steady) in the bus. CFD simulations were run until residuals became constant, for all

166 cases the iterations were over 100,000 times. Convergence was achieved after non-
 167 dimensional residuals for continuity equation, velocity components, energy, k and ε
 168 were below 10^{-3} , 10^{-4} , 10^{-6} , 10^{-4} and 10^{-4} , respectively and the monitored variables at
 169 specific surfaces were stable. We also checked energy balance and mass balance to help
 170 determine the convergence.

171 **2.2.3. Droplet dispersion modeling**

172 After the steady airflow field calculation was solved, we started the simulation of
 173 tracer gas dispersion and particle tracking, separately. The second-order upwind scheme
 174 was adopted in the tracer gas simulation. The mass fraction of C_2H_6 in the index
 175 patient's exhalation flows was 0.32 in CFD simulations according to [Ou et al. \[11\]](#).
 176 Lagrangian method with the Discrete Phase Modeling (DPM) was adopted to simulate
 177 the droplet dispersion with initial diameters of 5 μm , 50 μm and 100 μm [\[28, 43\]](#).
 178 Lagrangian equations of the droplets for i direction are as follows:

$$179 \quad \frac{dx_{p,i}}{dt} = u_{p,i} \quad (1)$$

$$180 \quad \frac{du_{p,i}}{dt} = \sum F_i = F_{drag,i} + F_{g,i} + F_{a,i} \quad (2)$$

$$181 \quad F_{drag,i} = \frac{f_D}{\tau_p} (u_i - u_{p,i}) \quad (3)$$

$$182 \quad F_{g,i} = \frac{g_i}{\rho_p} (\rho_p - \rho) \quad (4)$$

183 where $x_{p,i}$ and $u_{p,i}$ are the droplet displacement (m) and velocity (m/s) in i direction,
 184 respectively; $F_{drag,i}$ is the drag force ([Eq. \(3\)](#)), $F_{g,i}$ is the gravitational force ([Eq. \(4\)](#)). In
 185 addition, $F_{a,i}$ is the additional forces ([Eq. \(2\)](#)) for which we only considered Brownian
 186 force and Saffman's lift force [\[28, 44\]](#). ρ_p and ρ are the density of droplets and air,

187 respectively. f_D is the Stoke's drag modification function of Reynolds number for large
188 aerosol (Re_p) [45].

$$189 \quad f_D(Re_p) = 1 + 0.15 Re_p^{0.687} \quad (5)$$

190 In Eq. (3), τ_p is the aerosol characteristic response time, which is defined as:

$$191 \quad \tau_p = \frac{\rho_p d_p^2 C_c}{18\mu_t} \quad (6)$$

192 where μ_t is the turbulent viscosity ($\text{kg m}^{-1}\cdot\text{s}^{-1}$) and d_p is the droplet diameter. C_c is
193 the Cunningham slip correction factor, which is defined as [46]:

$$194 \quad C_c = 1 + \frac{2\lambda}{d_p} [1.257 + 0.4 \exp(-\frac{1.1d_p}{2\lambda})] \quad (7)$$

195 where λ is the molecular mean free path of air.

196 In CFD simulations, the mass ratio of liquid (water) and solid element (sodium
197 chloride) in droplets is assumed as 9 [47]. The densities of water liquid and sodium
198 chloride are respectively 998.2 kg/m^3 and 2170 kg/m^3 . The evaporation process will
199 continue until the droplets' volatile composition (i.e., water) is completely consumed.
200 The vaporization rate is governed by the gradient of the vapor concentrations between
201 the droplet surface and the bulk gas. The molar flux of vapor is defined as:

$$202 \quad N_i = k_c (C_{i,s} - C_{i,sr}) \quad (8)$$

203 where k_c is the mass transfer coefficient (m/s) which can be obtained by Sherwood
204 relationship [48]. The vapor concentrations at both droplet surface $C_{i,s}$ ($\text{kg}\cdot\text{mol}\cdot\text{m}^{-3}$)
205 and bulk air $C_{i,sr}$ ($\text{kg}\cdot\text{mol}\cdot\text{m}^{-3}$) are calculated by the assumption of the ideal gas.

Table 2

Boundary condition setups in CFD simulation.

Boundary name	Boundary condition
Skylight inlet	Velocity inlet , velocity is different with various running conditions (idling: 0.57 m/s, low bus speed: 2.09 m/s, high bus speed: 5.37 m/s), temperature is 11 °C, turbulent intensity is 5 %.
Skylight outlet	Outflow , velocity is same as skylight inlet, temperature is different with various running conditions (idling: 24 °C, low bus speed: 23 °C, high bus speed: 21 °C), turbulent intensity is 5 %.
Glass at wall surface	No slip wall , heat flux is determined by energy balance estimates (idling: 92.89 W/m ² , low bus speed: 79.00 W/m ² , high bus speed: 56.63 W/m ²).
Index-patient side radiator	Standard wall function, no slip wall , heat flux is 100 W/m ² , surface area is 3.38 m ² .
Opposite side radiator (closed)	Standard wall function, no slip wall , heat flux is 0 W/m ² , surface area is 3.38 m ² .
Wall of bus, luggage rack, seat	Standard wall function, no slip wall , heat flux is 0 W/m ² .
Nose (except index patient)	Mass-flow-outlet , mass flow rate is 9.23×10^{-5} kg/s, Nostril area is 2.87×10^{-4} m ² .
Mouth of index patient	Velocity inlet , exhaled airflow velocity is 1.5 m/s (in a direction paralleling to Y-axis), temperature is 32 °C.
Other body surface	Standard wall function, no slip wall , convective heat is 50 W for each person.

207

208 [Table 2](#) shows the relevant boundary condition settings in CFD simulations [11].

209 At the skylight inlet, the ambient air temperature was set as 11 °C, and the inlet velocity

210 was set as 0.57, 2.09 and 5.37 m/s according to the measured *ACH*. At the skylight

211 outlet, the air temperature was set as 24, 23, 21 °C according to the experiment. Non-

212 slip wall with standard wall function was applied at all wall surfaces. The effects of

213 human respiration and body surface heat fluxes were considered, with convective heat

214 fluxes of 50 W for each sedentary passenger. To simplify the calculations, it was

215 assumed that the droplets were exhaled from the mouth of the index patient, while the

216 other passengers only inhaled through noses. A value of heat flux determined by the
217 energy balance estimates was set on the bus window glasses [11].

218 After the steady airflow field with water vapor was solved, the single-diameter
219 droplets were uniformly released from the mouth of the index patient at a rate of 20
220 droplets per time step ($t = 0.1$ s, 18,000 iterations in total). The initial velocity of exhaled
221 droplets was 1.5 m/s and the initial temperature was 32 °C. After 30 min continuous
222 releasing, we got a fully-developed droplet distribution with a total droplet number of
223 360,000. When a droplet encountered a surface, it would have three different fates: trap,
224 reflect and escape. As shown in Table 3, different droplet sizes, surface roughness and
225 other factors would lead to different boundary conditions of droplets on the surfaces
226 [28, 49]. The trap condition was utilized for the floor, human surfaces and seats, which
227 means droplets were trapped once they touched the objects and the trajectory
228 calculations were terminated. While for the glass, roof, luggage racks and vertical walls,
229 the reflect condition was applied due to smooth surfaces or gravity, which means
230 droplets rebound off the surface and continue dispersion [28, 44, 50]. Escape condition
231 was adopted to the skylight outlet and passengers' noses (except the index patient).
232 Some of the CFD simulations in this study were completed on the Tianhe II
233 supercomputer with the support of the National Supercomputer Center in Guangzhou.

Table 3

Boundary conditions of each boundary in Discrete Phase Model.

Boundary name	Boundary conditions
Skylight, nose of passenger (except index patient)	Escape (trajectory calculations terminated)
Glass at wall surface, roof, luggage rack, vertical wall	Reflect (droplets suspended in air)
Floor, air conditioning, radiator, human body surface, seat	Trap (trajectory calculations terminated)

234

235 **2.3. Calculation of infection risk**

236 We adopted the Wells-Riley equation to calculate each passenger's infection risk
237 of aerosol inhalation transmission, which represented the probability of infection
238 through inhaling PLD. This method has been verified to effectively predict the infection
239 risk [51-53]. The Wells-Riley equation is defined as follows [54]:

$$240 \quad P = \frac{C_{infected}}{S_{susceptible}} = 1 - e^{-\frac{Iqpt}{Q}} = 1 - e^{-N_S} \quad (9)$$

241 where P is the probability of infection risk; $C_{infected}$ is the number of infected cases;
242 $S_{susceptible}$ is the number of susceptible people; I is the number of people in the infectious
243 stage or infectors; q is the quanta of PLD produced per infector per second (quanta/s);
244 p is the pulmonary ventilation rate of each susceptible (m^3/s); Q is the room ventilation
245 rate with virus-free air (m^3/s); t is the exposure time (s); N_S is the number of PLD
246 inhaled by susceptible person, which was calculated for droplets and tracer gas by using
247 different equations.

248 For droplets, N_S is defined as [54]:

$$249 \quad N_s(x, t_0) = C_v p \int_0^{t_0} C_d(t) dt = C_v N_i \quad (10)$$

250 where C_v is the concentration of the virus in the exhaled droplets; $C_d(t)$ is the quanta
251 concentration in an indoor environment at the time t (quanta/ m^3); t_0 is the exposure
252 period; N_i is the total number of droplets (exhaled from the index patient) inhaled by
253 passengers.

254 For tracer gas, N_S is defined as Eq. (11) according to the dilution-based
255 evaluation method [55]:

$$256 \quad N_s = \int_0^{t_0} p C_{g,q}(t) dt \quad (11)$$

257 where $C_{g,q}$ is the airborne quanta concentration at the target position (quanta/m³), and
258 defined as $C_{g,q} = \frac{qC_{g,p}}{p_s C_{g,s}}$, where p_s is the breathing rate of the infector (m³/s); $C_{g,s}$ and $C_{g,p}$
259 are the airborne contaminant concentrations (ppm) at the source and target position,
260 respectively.

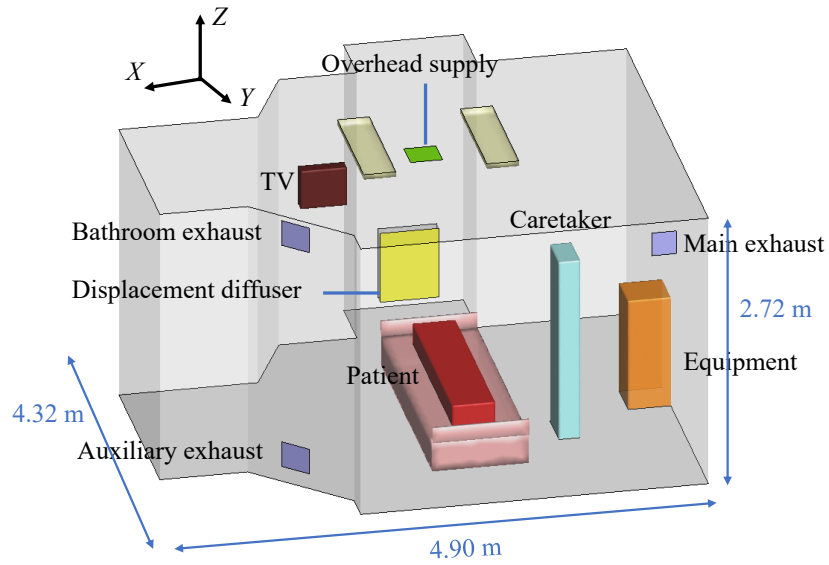
261 Despite a critical parameter for calculating the infection risk, the value of q from
262 a COVID-19 infector is currently not officially established. In this realistic bus outbreak,
263 there were one infector ($I = 1$) and 45 susceptible passengers ($S_{susceptible} = 45$), seven of
264 whom were infected ($C_{infected} = 7$). According to the travel history, this bus drove for
265 145 min at high speed ($Q = 5.69$ m³/min, $t = 145$ min), 45 min at low speed ($Q = 2.28$
266 m³/min, $t = 45$ min) and 10 min at idling ($Q = 0.62$ m³/min, $t = 10$ min). Substituting
267 these data into Eq. (9) could back-calculate the value of q as 0.61 min⁻¹ (36.6 h⁻¹). This
268 value agrees well with the range of 14–48 h⁻¹ obtained by Dai and Zhao [56] who
269 adopted a reproductive number-based fitting approach.

270 Ansys FLUENT was employed to simulate the number of droplets inhaled by each
271 passenger (N_i) and the concentration of tracer gas ($C_{g,s}$ and $C_{g,p}$). Then the N_s for
272 droplets and tracer gas were respectively obtained by Eq. (10) and Eq. (11). Finally, the
273 infection risk of each passenger was calculated by Eq. (9) for both droplets and tracer
274 gas. In order to compare the infection risk under various ventilation rates, we carried
275 out a 30-minute simulation for each vehicle driving situation.

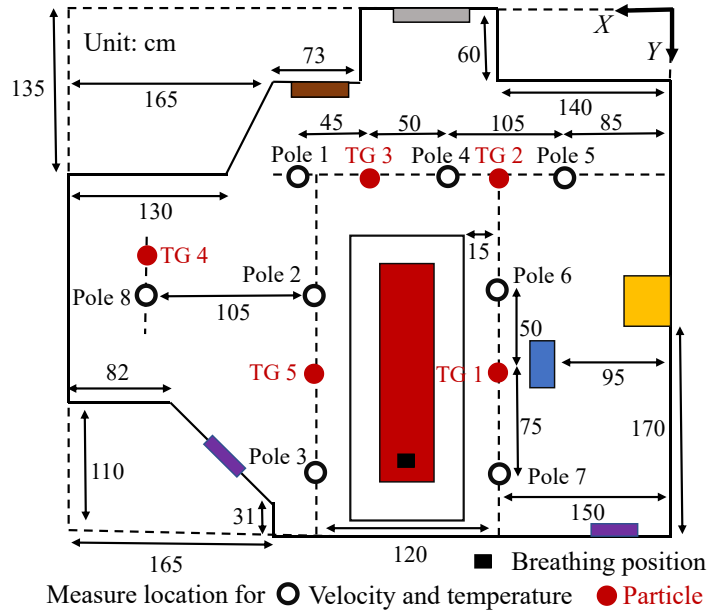
276 **2.4. Validation of numerical modeling**

277

278



(a)



(b)

Fig. 2. Model setups of single-bed isolation room in CFD validation case (Yin et al., 2009).

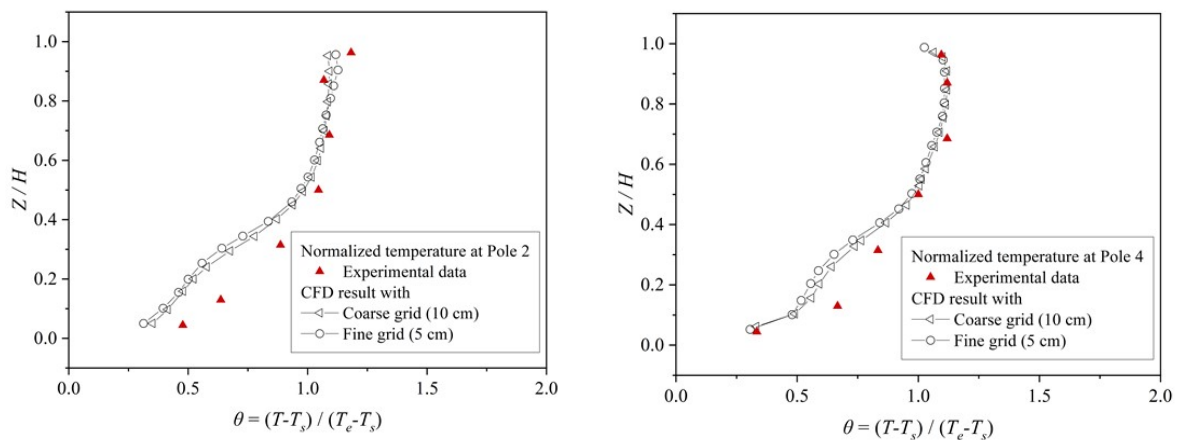
279

280 Firstly, we performed a set of dispersion tests for validating the CFD predictions
 281 of tracer gas dispersion. The evaluation of tracer gas dispersion by this field
 282 experimental data can refer to our previous study [11].

283 In addition, we further carried out a validation study of indoor airflows,
 284 temperature and tracer gas/particle dispersion in a hospital ward evaluated by the
 285 experiment conducted by Yin et al. [36]. As shown in Fig. 2a, the experiment was
 286 performed in a full-scale one-person patient ward (4.90 m × 4.32 m × 2.72 m). The
 287 ventilation rate from the displacement diffuser was 0.054 m³/s (4 ACH) and the
 288 temperature was 19.5 °C. The ventilation rates of bathroom exhaust and main exhaust
 289 were 0.017 m³/s and 0.037 m³/s, respectively. As shown in Fig. 2b, the air velocity and
 290 temperature were measured at seven heights of Poles 1-8. Particle concentration was
 291 measured at poles TG1 - TG5 at six heights. More details about the experimental setups
 292 could be found in Yin et al. [36].

293 In this validation, we adopted 1.8 million and 3.8 million tetrahedral grid cells with
 294 fine and coarse grid resolutions, respectively. Then, we selected the measured vertical
 295 profiles of normalized velocity (V/u_s , $u_s = 0.14$ m/s means the supply air velocity) and
 296 temperature ($\theta = (T-T_s)/(T_e-T_s)$) at Pole 2 and Pole 4 to validate CFD results, where T_s
 297 and T_e are the temperatures respectively at diffuser and main exhaust at the normalized
 298 height (Z/H , $H = 2.72$ m is the height of the inpatient ward).

299



(a)

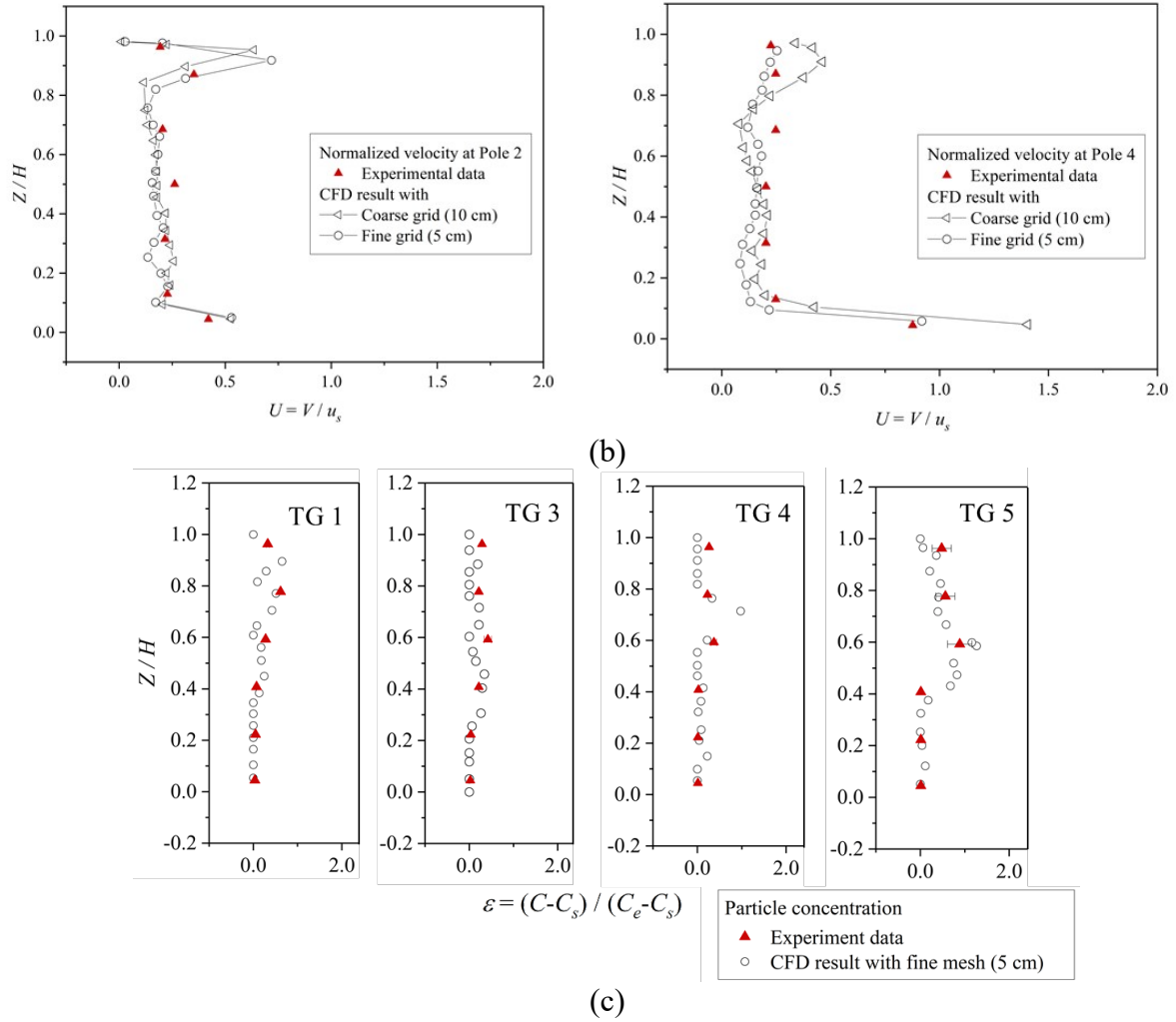


Fig. 3. Vertical profiles of experiment and CFD simulation at Pole 2 and Pole 4 (a) Normalized temperature, (b) Normalized velocity; (c) Normalized 1 μm particle concentration at TG 1, TG 3, TG 4 and TG 5.

300

301 [Fig. 3a-b](#) illustrate that CFD results of velocity and temperature agree well with
 302 the experimental data. Compared with the coarse grid resolution, fine grid resolution
 303 performs better, especially in the velocity at height of $Z/H = 0.8$. [Fig. 3c-f](#) display the
 304 experimental data and CFD simulation results of normalized particle concentration ε at
 305 TG1, TG3, TG4 and TG5 ($\varepsilon = (C - C_s) / (C_e - C_s)$, where C , C_s and C_e are the particle
 306 concentrations at the measuring location, ventilation supply inlet and ventilation
 307 exhausts, respectively). Particles with a diameter of 1 μm are released from the patient's

308 mouth. In order to quantify the reliability of the validation, we calculated the
309 normalized mean square error (NMSE) and fractional bias (FB), whose ranges were
310 respectively 0.3 to 1.3 and 0.01 to 0.27, which satisfied the recommended criteria
311 (($NMSE \leq 1.5$, $0.3 \leq FB \leq 0.3$) in Yang et al [57]. The results indicate that CFD
312 simulation results can reasonably predict the dispersion tendency of indoor particles.

313

314 **3. Results**

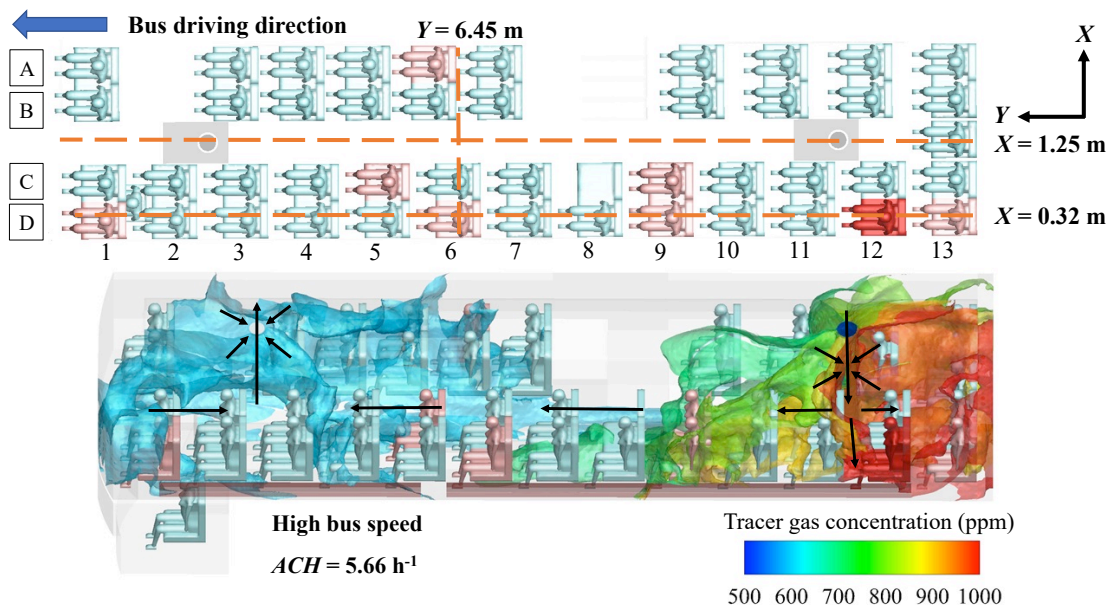
315 ***3.1. Flow pattern and tracer gas dispersion under various ACH***

316 Our previous study [11] only considered the tracer gas dispersion under the
317 measured mean ventilation condition. In the present study, we emphasize the flow
318 pattern and tracer gas dispersion under different ventilation conditions (i.e., $ACH = 0.62$,
319 2.27 and 5.66 h^{-1}).

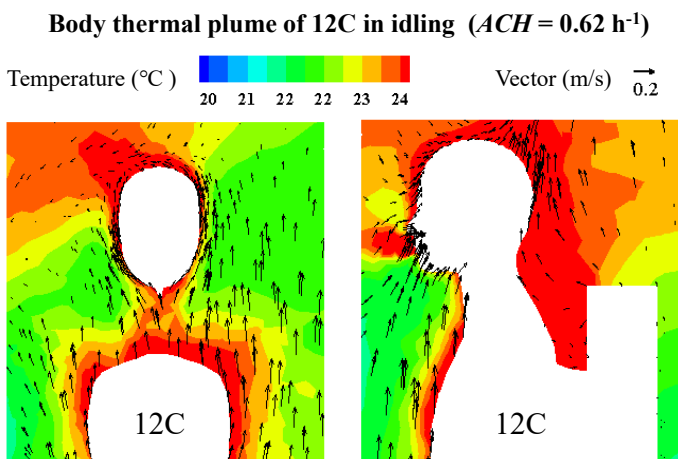
320 In order to describe the flow pattern and tracer gas dispersion more clearly, seat
321 locations are shown in Fig. 4a: 13 rows (Row 1-13) and 5 columns (Column A, B, C,
322 D, E) of seats in the passenger cabin. We regard the 1st to 4th rows as the bus front, the
323 5th and 8th rows as the bus middle and the 9th to 13th rows as the bus rear. The index
324 patient is located at seat 12D (Row 12, Column D, scarlet).

325 Fig. 4a indicates that when the bus speed is high ($ACH = 5.66 \text{ h}^{-1}$), the fresh air
326 enters the skylight inlet at the rear roof, then mixes with the dirty air and moves from
327 the rear to the front. Finally, the mixed air leaves through the outlet at the front roof of
328 the bus. There are body thermal plumes which lead to significant upward airflow near
329 and above human bodies (Fig. 4b). The upward airflow will intertwine with the main
330 flow field and subsequently affect the droplet dispersion. Fig. 4c displays that the

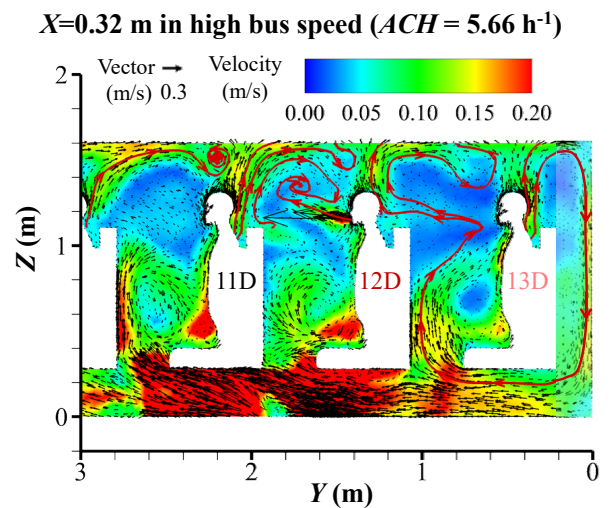
331 airflow exhaled by the index patient first moves forward, then rises up and finally
 332 deflects backward to the bus rear. As depicted in Fig. 4d, the body thermal plumes are
 333 most obvious under idling condition ($ACH = 0.62 \text{ h}^{-1}$). The ventilation flow from bus
 334 rear to bus front enhances significantly as ACH rises with the increasing bus speed (Fig.
 335 4e).
 336



(a)

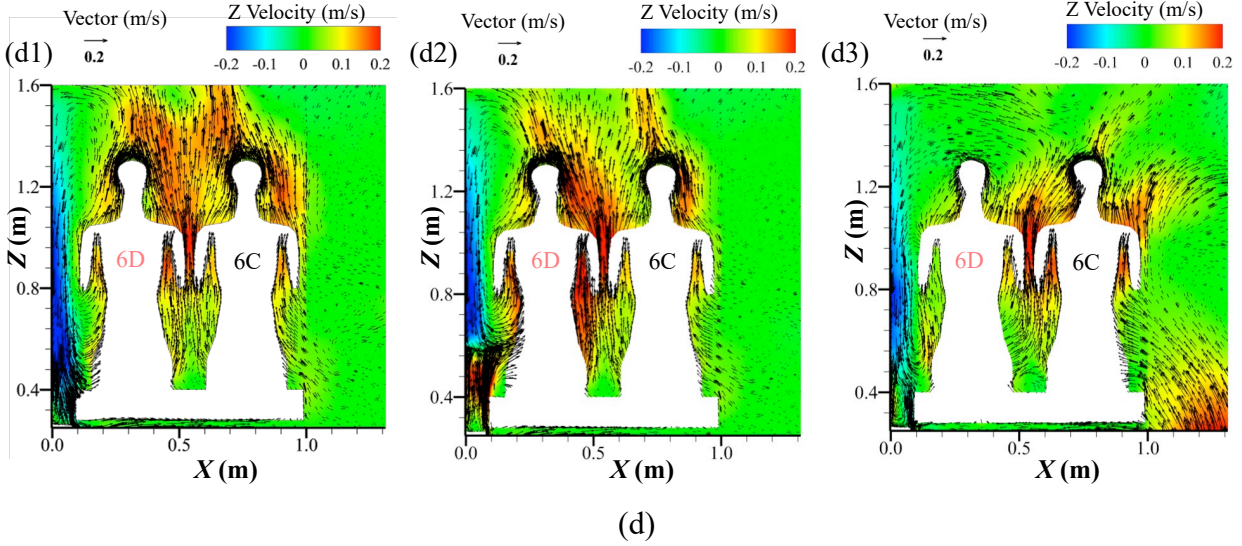


(b)

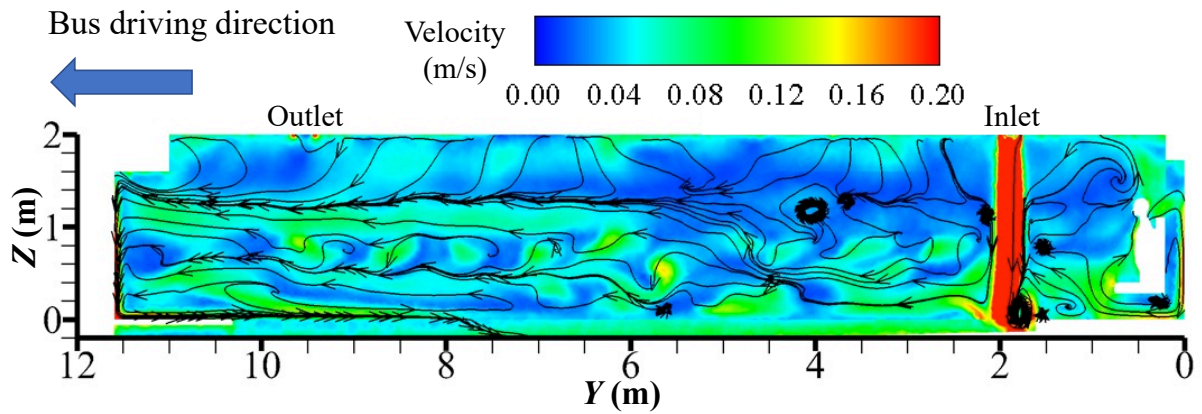


(c)

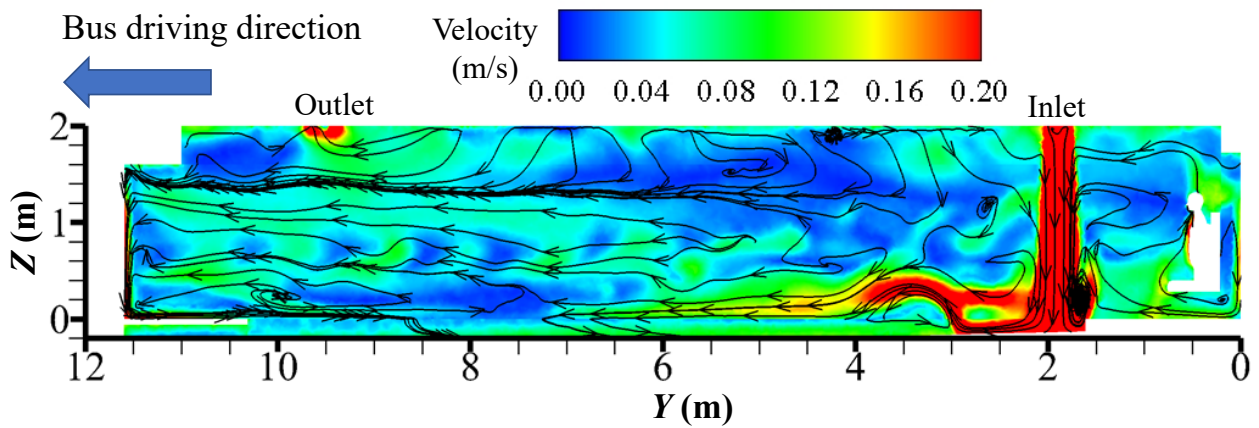
$Y=6.45$ m in idling ($ACH=0.62$ h⁻¹) $Y=6.45$ m in low bus speed ($ACH=2.27$ h⁻¹) $Y=6.45$ m in high bus speed ($ACH=5.66$ h⁻¹)



(e1) $X = 1.25$ m in idling ($V_{Bus} = 0$ km/h, $ACH = 0.62$ h⁻¹)



(e2) $X = 1.25$ m in low bus speed ($V_{Bus} = 30$ km/h, $ACH = 2.27$ h⁻¹)



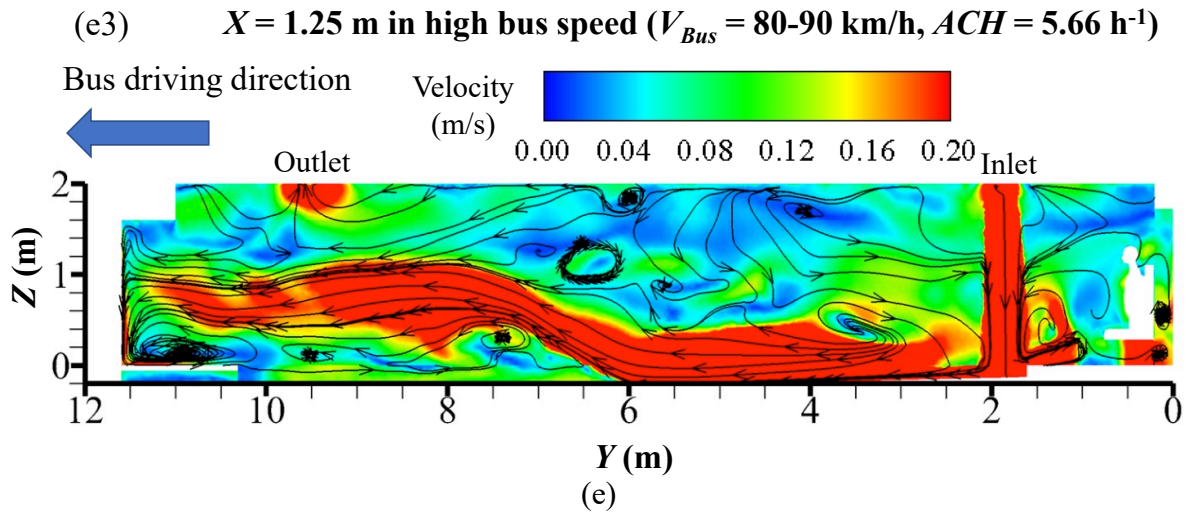


Fig. 4. (a) Cross-section line and general flow characteristics; (b) Body thermal plume of 12C at state of idling; (c) Flow field near index patient at state of high bus speed; Flow field in Plane: (d) $Y = 1.35$ m; (e) $X = 1.25$ m. 1-3: idling, low bus speed, high bus speed, respectively.

337

338 [Fig. 5](#) presents the tracer gas concentration distribution of the cross-section at the
 339 height of passengers' noses ($Z = 1.16$ m) under different ACH . Tracer gas concentration
 340 in the bus decreases obviously when ACH increases. High tracer gas concentration
 341 mainly appears in the bus rear (Rows 9-13), especially at the index patient's side
 342 (Columns C and D). Particularly when $ACH = 0.62$ h⁻¹, the concentration near the index
 343 patient is about 7000 ppm, and 5000 ppm in the bus front and middle (Rows 1-8) ([Fig.](#)
 344 [5a](#)). When $ACH = 5.66$ h⁻¹, the concentration near the index patient is about 1200 ppm,
 345 while around 600 ppm in the bus front and middle. ([Fig. 5c](#)).

346

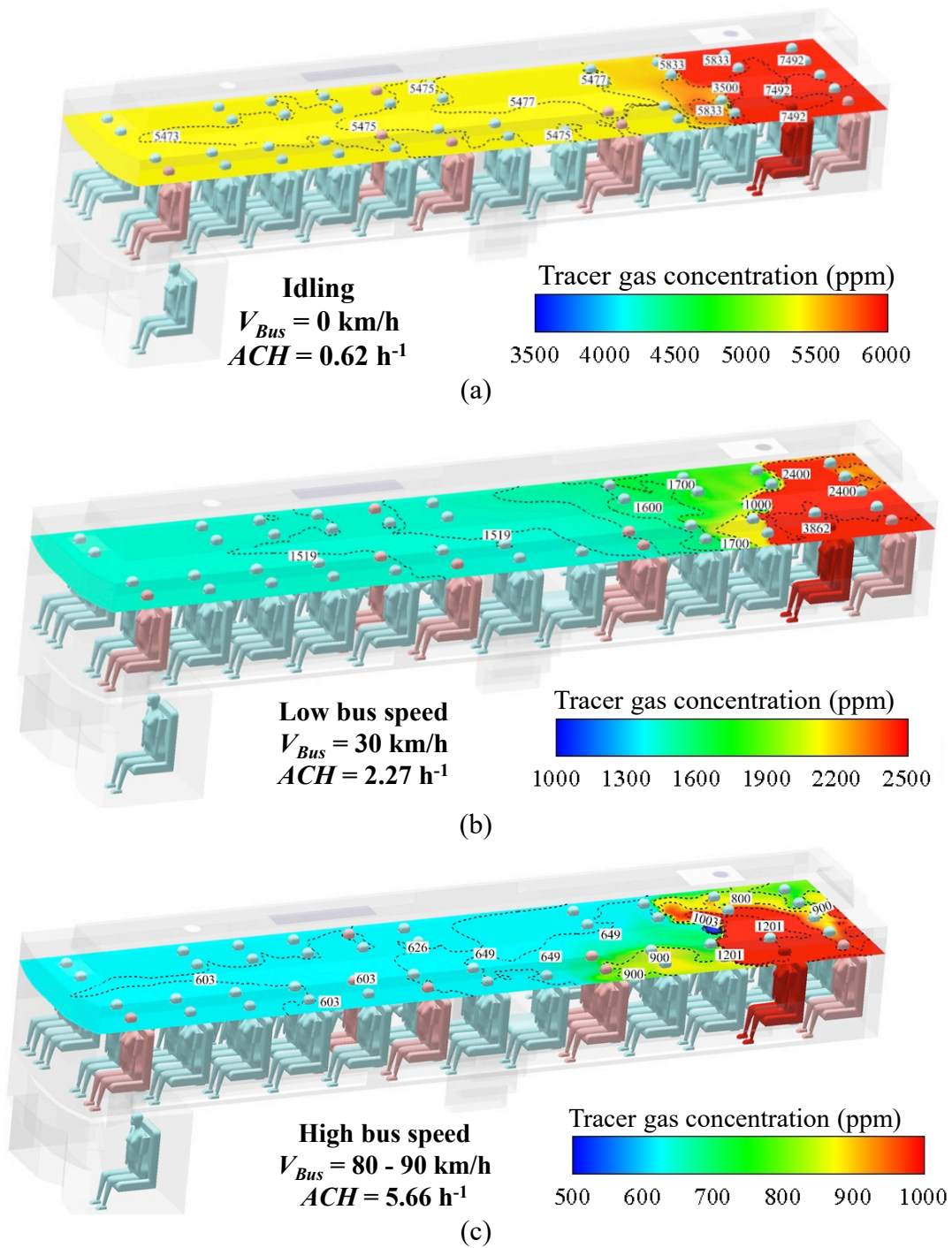


Fig. 5. Tracer gas concentration at state of: (a) idling, (b) low bus speed; (c) high bus speed.

348 **3.2. Impacts of RH, ACH and initial diameters on droplet dispersion**

349 **3.2.1. Impacts of RH on droplet evaporation and transmission**

350 **Fig. 6** displays the temporal variation of droplet diameters (droplet evaporation
351 history) under different RH (35%, 95%) when initial diameter d_p is 50 μm and 100 μm .
352 When $d_p = 5 \mu\text{m}$, droplets can evaporate into 1.83 μm nuclei within 0.1 s under both
353 RH conditions, so we don't show its evaporation process here. The results confirm that
354 50 μm droplets can evaporate into 18.26 μm droplet nuclei in 1.3 s under RH = 35%
355 and 2.1 s under RH = 95%. However, it takes 5 s for 100 μm droplets to evaporate into
356 36.50 μm nuclei under RH = 35% and longer time (> 6 s) under RH = 95%. Although
357 droplets take a longer time to evaporate in more humid environment, the overall impact
358 of RH is not significant in this coach bus with complicated interactions of ventilation
359 airflow and thermal body plumes (Fig. S1).

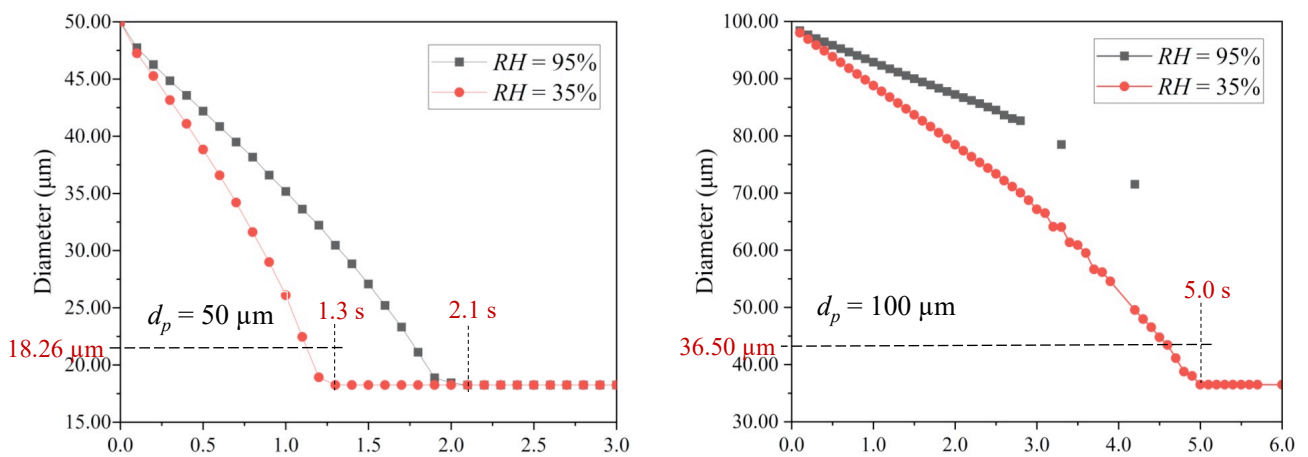


Fig. 6. Temporal variation of droplet evaporation ($d_p = 50 \mu\text{m}$, $100 \mu\text{m}$; RH = 35%, 95%).

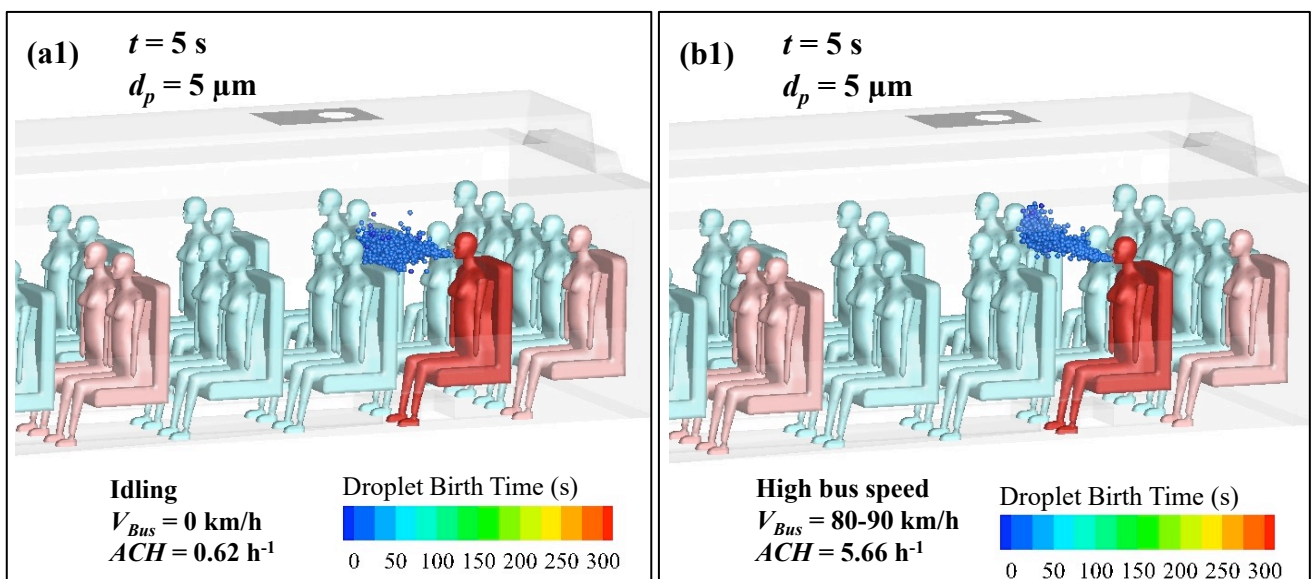
360

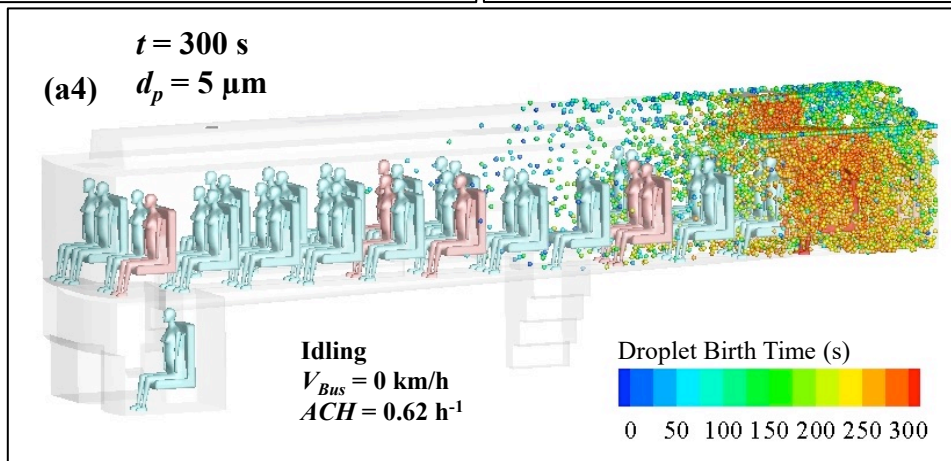
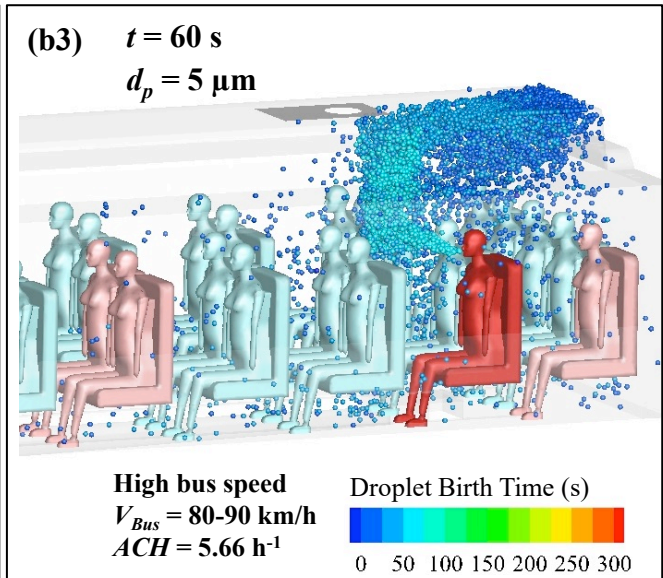
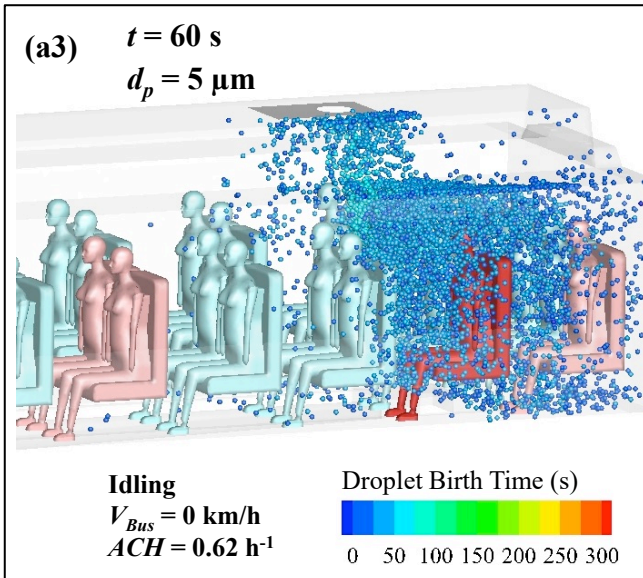
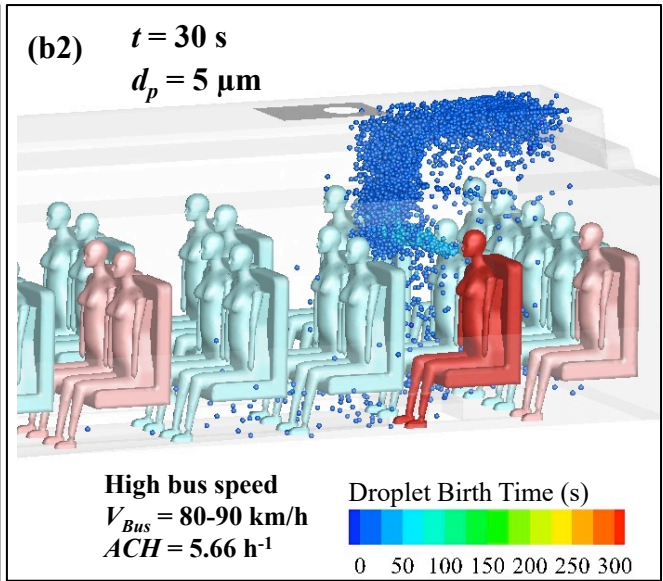
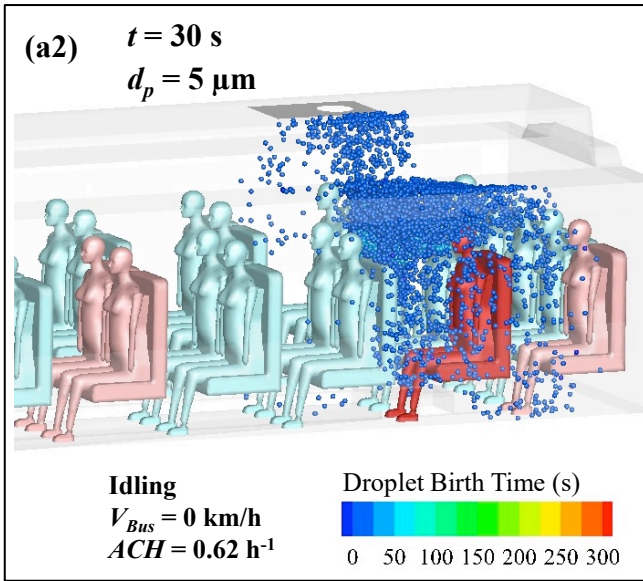
361

362 **3.2.2. Impacts of ventilation rates on droplet dispersion**

363 We have investigated the impacts of ventilation rates on the dispersion of droplets
364 in different initial diameters (5 μm , 50 μm and 100 μm), and find that the dispersion
365 mechanism is more affected by the gravity force and less influenced by the ventilation
366 airflow for larger droplets. Thus, to better reveal the influence of ventilation rates, we
367 only select 5 μm droplets to display their distribution under $RH = 35\%$ at $t=5\text{s}$, 30 s, 60
368 s and 300 s with three ACH , as shown in Fig. 7.

369 As verified in Fig. 7a1-b1, after being exhaled by the index patient, droplets first
370 move forward due to the initial exhalation flow, then rise up following the upward flow
371 near the index patient, and spread with the main airflow routes (Fig. 7a2-b2). Due to
372 the variation in ventilation rates, the spatial distribution of droplets also differs
373 significantly (Fig. 7a3-a4). When $ACH = 5.66 \text{ h}^{-1}$ with larger supply airflow blowing to
374 the bus front, more droplets move forward and escape from the skylight outlet, leaving
375 relatively fewer droplets in the bus rear (Fig. 7a4-b4). The results show that increasing
376 the ventilation rate is beneficial to droplet dilution and excretion, and significantly
377 reduces the droplet concentration near the index patient (i.e., seats 11D, 12C and 13D).





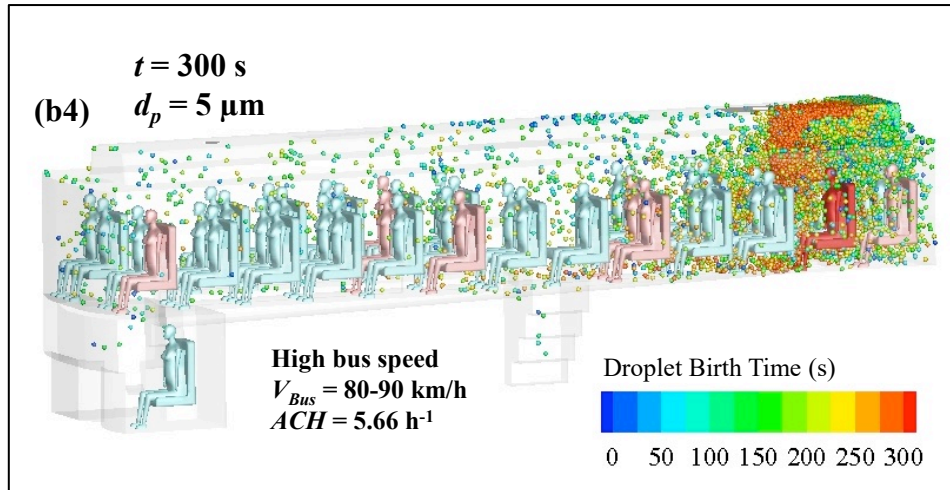


Fig. 7. Distribution of 5 µm droplets with $RH = 35\%$ at state of: (a) idling, (b) high bus speed.

378

379 3.2.3. Impacts of droplet initial diameters on droplet dispersion

380 Fig. 8 indicates the evaporation and dispersion of droplets with different initial
 381 diameters when $RH = 35\%$ and $ACH = 2.27 \text{ h}^{-1}$. 5 µm droplets can evaporate rapidly
 382 into nuclei, so they are more significantly affected by the airflow field, and spread wider
 383 in the whole bus (Fig. 8a1-a3). Due to the combined action of airflow pattern and
 384 gravity force, 50 µm droplets mainly concentrate at the bus rear (Fig. 8b1-b3). With the
 385 dominance of gravity force, 100 µm droplets rapidly settle down from the exhalation
 386 jet after being exhaled from the index patient's mouth (Fig. 8c1-c3). Basically, the larger
 387 the initial diameter is, the quicker the droplets deposit, and hence the smaller range they
 388 propagate and the more they remain in the bus.

389

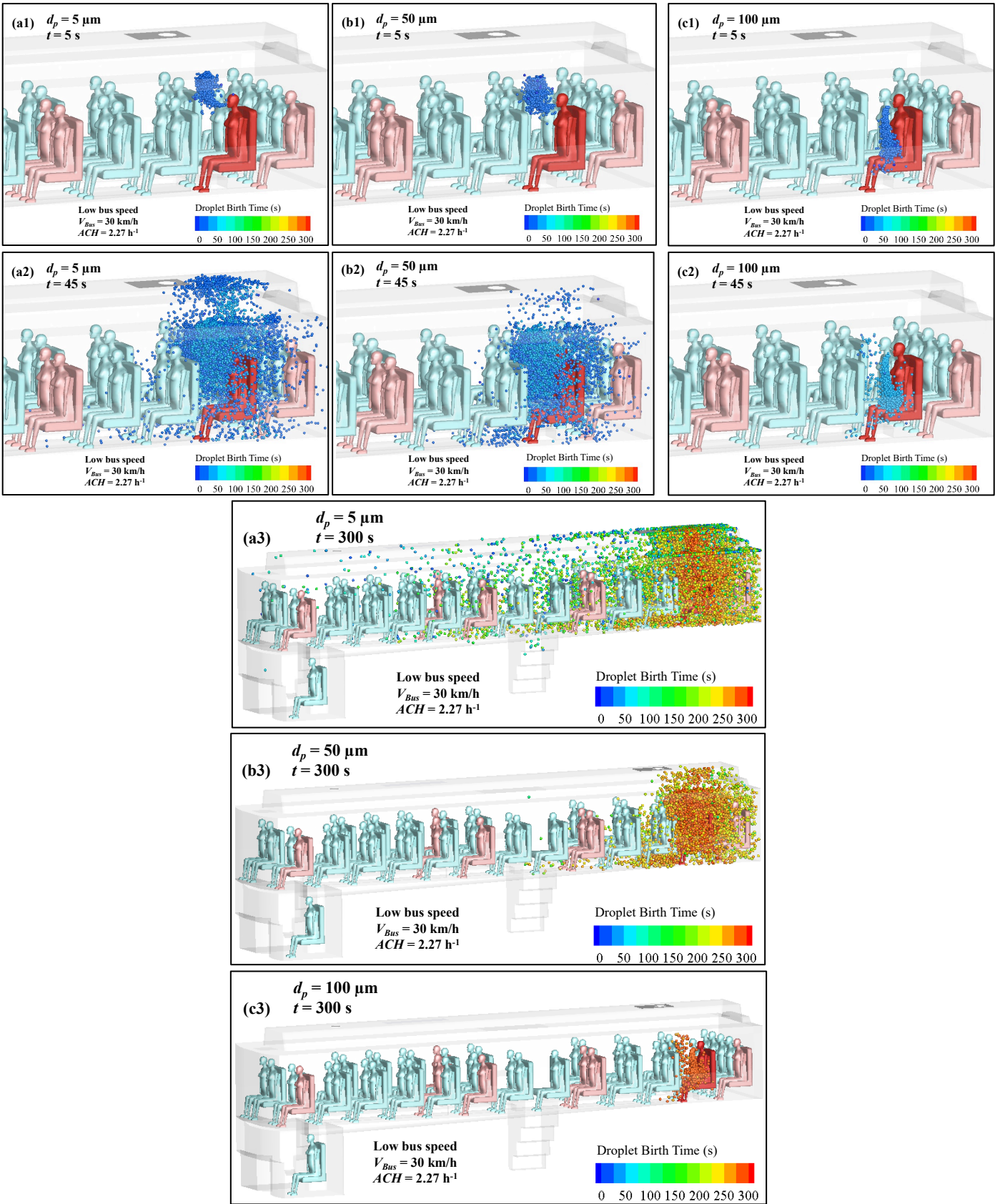


Fig. 8. Droplets distribution in low bus speed with $RH = 35\%$: (a) $d_p = 5 \mu\text{m}$, (b) $d_p = 50 \mu\text{m}$, (c) $d_p = 100 \mu\text{m}$.

390 3.3. Intake fraction and infection risk of each passenger

391 Fig. 9 depicts the 30-minute-exposure intake fraction (*TIF*) of each passenger
392 which is defined as dividing the number of droplets a passenger inhaled by the total
393 number of droplets released from the index patient (360,000). Fig. 10 depicts the 30-
394 minute-exposure infection risk (*TIR*) of each passenger which is calculated by Wells-
395 Riley equation (Eq. (9)). The *X*-axes represent the row of each passenger, where 12D is
396 the location of the index patient and 8C is unoccupied. Passengers without data indicate
397 that they did not inhale PLD released by the index patient.

398 For 5 μm droplets, the ventilation rates influence the *TIF* and the subsequent *TIR*,
399 with a higher ventilation rate leading to more passengers at *TIR*. When $ACH = 0.62 \text{ h}^{-1}$,
400 only few 5 μm droplets are inhaled by passengers in the bus front (Fig. 9a), leading
401 to most front passengers at no droplet *TIR* (Fig. 10a). When ACH increases to 5.66 h^{-1} ,
402 even more front passengers are at *TIR*, and both *TIF* and *TIR* of passengers decrease
403 with the distance between the passenger and index patient (Fig. 9c). Although 5 μm
404 droplets disperse more widely with the increasing ventilation, the *TIR* is quite low
405 ($<0.01\%$) for front passengers. Regardless of ventilation rate, more than 97% of 50 μm
406 droplets deposit near the index patient due to gravity (Table. S1), so only the middle
407 and rear passengers are at *TIR* with the highest infection risk for passenger 12C (3.13%
408 under $ACH = 5.66 \text{ h}^{-1}$) (Fig. 10b). While for 100 μm droplets, over 99.5% of them
409 deposit locally due to gravity (Table. S1), making nobody at *TIF*, so we don't display
410 the infection risk.

411 For the tracer gas, a higher ventilation rate leading to lower *TIR*. The *TIR* is 11.10-
412 15.29% under $ACH = 0.62 \text{ h}^{-1}$, and decreases to 1.27-3.09% when $ACH = 5.66 \text{ h}^{-1}$ (Fig.

413 10c). The *TIR* of tracer gas for each passenger is more uniform and distinctly higher
 414 under the same condition, compared with that of droplets.

415

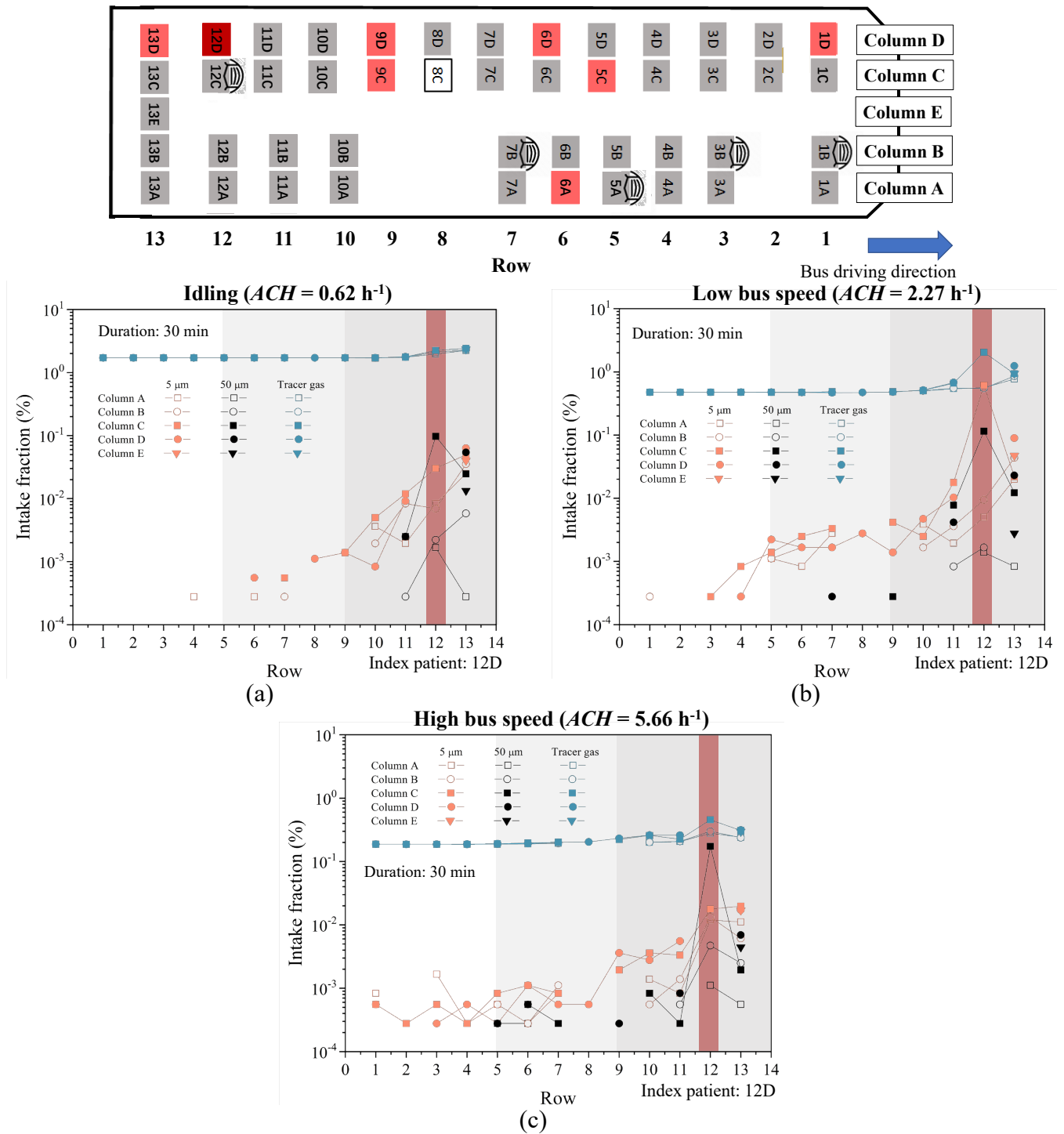


Fig. 9. Intake fraction of each passenger in a duration of 30 min under $RH = 35\%$ at state of: (a) idling, (b) low bus speed, (c) high bus speed.

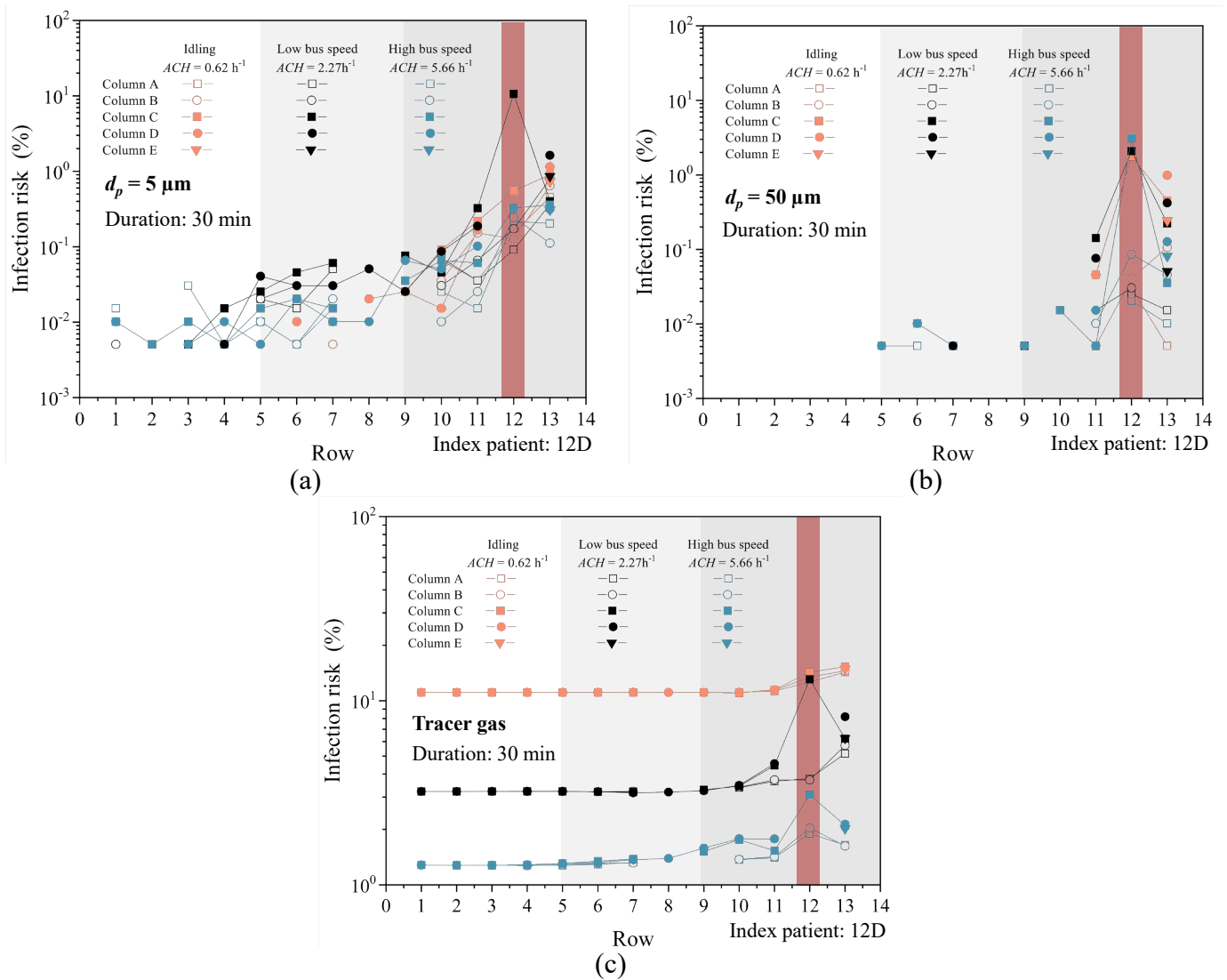


Fig. 10. Infection risk of each passenger under $RH = 35\%$: (a) $d_p = 5 \mu\text{m}$, (b) $d_p = 50 \mu\text{m}$, (c) tracer gas. (Note: infection risk within 30 min was calculated.)

416

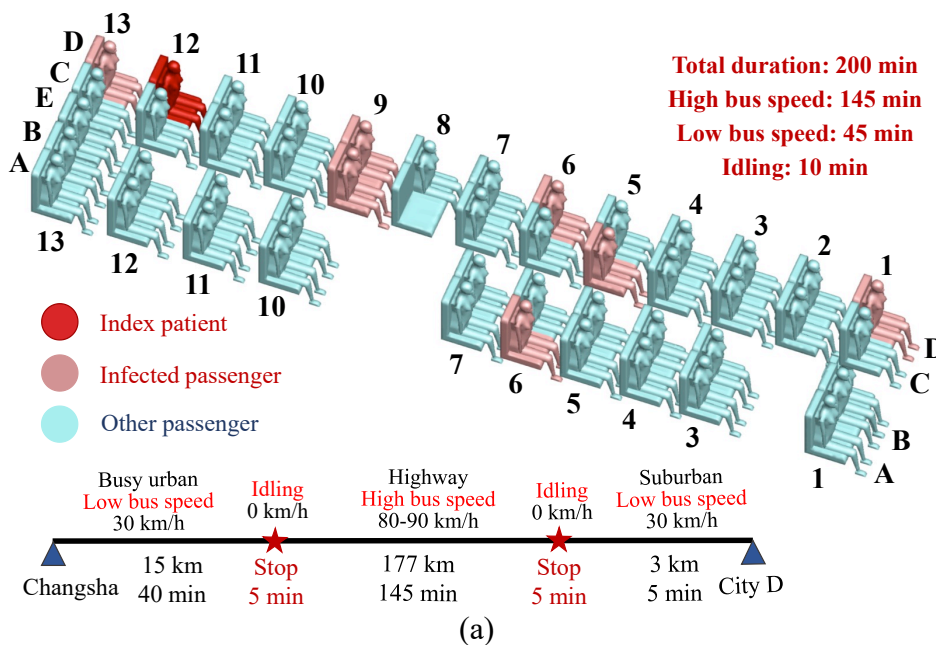
417 **3.4. Infection risk of each passenger in this epidemic outbreak**

418 The total duration of the bus journey is 200 min, and the passenger seating
 419 arrangement and driving route are depicted in Fig. 11a. We adopted the calculated 30-
 420 minute simulation results to infer the quanta of virus-laden droplets or tracer gas inhaled
 421 by each passenger throughout the whole journey. Fig. 11b-11d display the whole-

422 journal-exposure infection risk (*WIR*) of passengers (except the index patient at seat
 423 12D). Note that the logarithmic coordinate system is employed in Fig. 11c-11d.

424 Under all conditions, the highest *WIR* of the tracer gas, 5 μm and 50 μm droplets
 425 occurs at seat 12C with 33.85%, 16.99% and 17.40%, and followed by seat 13D with
 426 24.97%, 4.28% and 1.57%, respectively. It can be seen from Fig. 11 that the *WIR* of
 427 front-seat passengers significantly decreases with the increasing initial droplet diameter.
 428 However, passengers near the index patient (i.e., seats of 11D, 12C and 13D) are always
 429 at comparatively high *WIR*.

430 For the tracer gas (Fig. 11b), the *WIR* of front passengers is relatively even at
 431 $\sim 14.00\%$. For 5 μm droplets (Fig. 11c), the *WIR* is quite discrepant for passengers at
 432 different locations, and is less than 0.15% for the front passengers (Rows 1-4), while
 433 up to 16.99% for the passenger at 12C. For 50 μm droplets (Fig. 11d), no front
 434 passengers are at *WIR*.



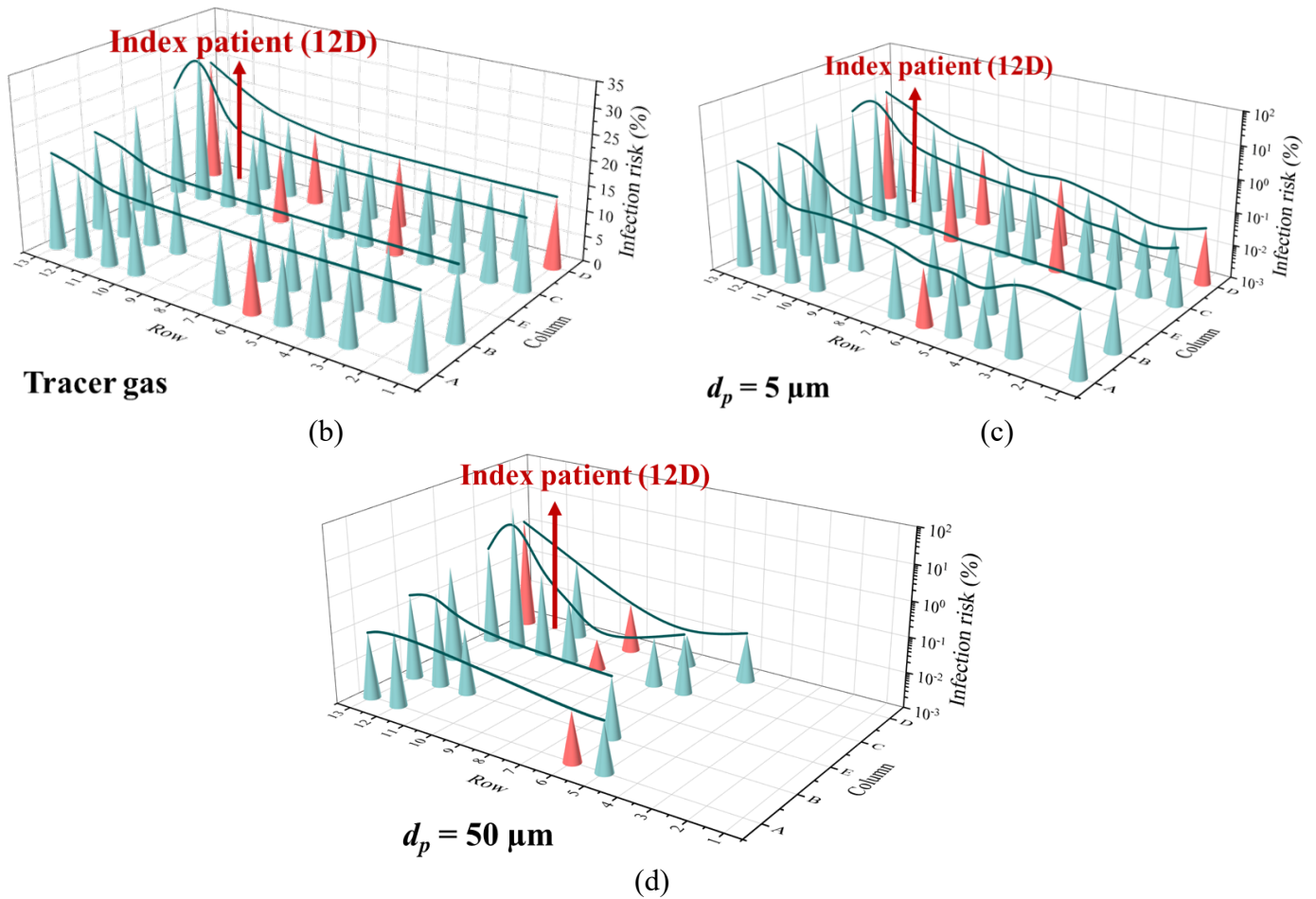


Fig. 11. (a) Seating arrangement, journeys, and distribution of index patient and infected passengers, (b) Tracer gas, (c) $d_p = 5 \mu\text{m}$, $RH = 35\%$, (d) $d_p = 50 \mu\text{m}$, $RH = 35\%$. (Note: infection risk is calculated based on this epidemic case.)

435 **4. Discussion**

436 *4.1. The unique airflow field characteristics of the coach bus*

437 The strength of this study lies in the investigation of the combined effect of the
 438 indoor main airflow and human thermal plumes on the airflow field in this unique in-
 439 coach environment. The coach bus only has small roof-opening skylight suppliers to
 440 open up for fresh air, but no windows are openable. Fig. 12 depicts the external surface
 441 wind pressure coefficient around the running bus. It shows that the pressure on the rear
 442 half is higher than the front half of the bus, which leads the air enter the bus from the

443 rear skylight and exit from the front, i.e., the indoor main airflow is moving from the
 444 rear to front. This unique rear-to-front airflow pattern makes the pathogen-laden
 445 expiratory droplets propagate the entire bus when the index patient is seated at the bus
 446 rear (12D) and hence results in large-scale transmission in this outbreak, as was also
 447 found in Mesgarpour et al. [58]. If the index patient was in the middle or front of the
 448 bus, the rear of the bus will be a low-risk area [59].

449

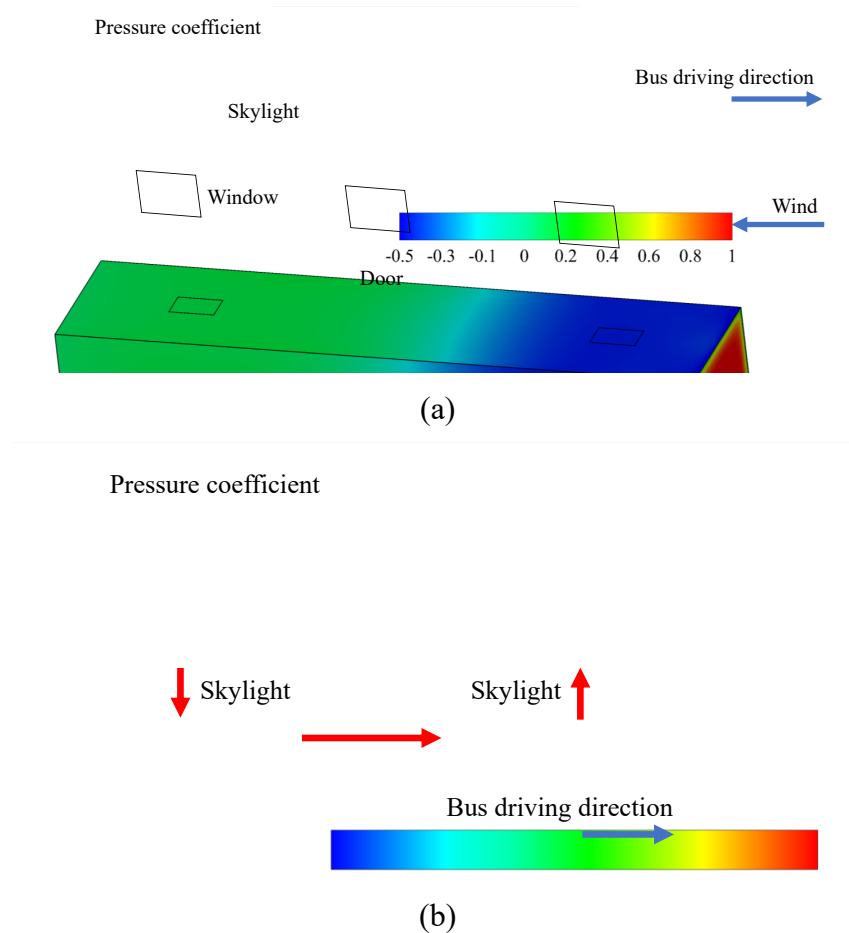


Fig. 12. (a) Pressure coefficient distribution on bus surfaces, (b) External pressure coefficient distribution of bus.

450

451 Besides the main airflow, the body thermal plumes cannot be neglected in the
452 crowded coach bus, as they can cause an upward airflow near each human body and
453 hence influence the droplet dispersion in the respiratory region—the last few inches for
454 aerosol transmission to effectuate [17, 22, 60]. Meanwhile, Yang et al. [61] found that
455 strong main airflow could destroy the thermal plumes. The body thermal plumes are
456 obvious under the small background velocity field and can inhibit droplets from
457 entering the respiratory area. This certain protective effect makes droplet infection risk
458 stay low under $ACH = 0.62 \text{ h}^{-1}$. However, the body thermal plumes will be disturbed
459 with the enhancement of the main airflow, leading to an increase of the droplet infection
460 risk under $ACH = 2.27 \text{ h}^{-1}$.

461 ***4.2. Impacts of RH and initial droplet diameter on droplet dispersion***

462 Redrow et al. [38] demonstrated that $10 \mu\text{m}$ droplets could evaporate completely
463 in 0.25 s at $RH = 20\%$ and 0.55 s at $RH = 80\%$, and RH influenced $0.4\text{-}10 \mu\text{m}$ droplet
464 transport in a simulated room where the mean air velocity was almost zero. Liu et al.
465 [17] revealed that $100 \mu\text{m}$ droplets took more than 100 s to evaporate at $RH = 95\%$ and
466 $<2 \text{ s}$ at $RH = 35\%$, which made $100 \mu\text{m}$ droplet dispersion totally distinct under different
467 RH in an empty room. However, our study achieved a completely different finding: RH
468 rarely influences the droplet ($5\text{-}100 \mu\text{m}$) dispersion in the coach bus. The possible
469 reason may lie in the complex indoor environment of the coach bus which is different
470 from those in the above literature. In our study, we found that the interaction of the main
471 airflow and body thermal plumes made the airflow much more complex, which
472 significantly influenced the droplet/tracer gas dispersion. Moreover, Chen and Zhao [62]

473 and Xie et al. [33] indicated that regardless of the RH , small droplets evaporated
474 completely quickly, and big droplets deposited downward immediately before fully
475 evaporating due to gravity dominance. Therefore, there was a tiny difference of droplet
476 ultimate fates and infection risk between different RH (Table. S1, Fig. S2), which agreed
477 well with the study on coach bus conducted by Yang et al. [28].

478 The droplet diameter is the fundamental property that determines its transport
479 characteristics. The transport behavior of a droplet depends on its interaction with the
480 surrounding gas molecules, as well as the force acting on it [63]. When the droplet
481 diameter increases, its dominant influencing mechanism changes into gravity force or
482 drag force [64, 65]. Zhu et al. [66] indicated that the droplets of 30 μm or smaller were
483 mostly influenced by indoor airflow, but those of 50 – 200 μm were significantly
484 affected by the gravity force. Our study found that small droplets (i.e., tracer gas and 5
485 μm droplets) can follow the airflow and spread throughout the cabin, while large
486 droplets (i.e., 50 μm and 100 μm) deposited near the index patient due to the dominant
487 gravity force. Namely, small droplets can travel farther than large droplets, leading to a
488 larger range of inhalation transmission.

489 When the droplet is small enough, the behavior of the droplets and the surrounding
490 gas requires the kinetic theory of gases. Therefore, tracer gas was adopted as a surrogate
491 for droplets and droplet nuclei smaller than 5 μm in general room environments, which
492 had been verified by existing studies [36, 44, 67]. However, unlike general rooms, buses
493 are longer and narrower in shape (11.4 m long and 2.5 m wide in our study) with more
494 obstacles (i.e., human bodies and seats), which provides much more surface for droplets
495 to deposit. Our study verifies that most droplets deposit on the route through the long-

496 and-narrow bus so that only a small fraction can spread to the bus front. Therefore,
497 passengers in the bus front can expose to few droplets and lead to a quite low infection
498 risk. However, tracer gas does not deposit and can disperse in the whole cabin, resulting
499 in distinctly higher infection risk under the same condition. Hence, tracer gas cannot be
500 utilized to mimic the dispersion processes of droplets which can be deposited on the
501 surfaces. Meanwhile, Zhao et al.[68] indicated that the deposition of 0.7 μm particles
502 was insignificant in an aircraft cabin. Lai and Nazaroff [69] reported that droplets in the
503 range of 0.1-0.2 μm has the lowest deposition rate in indoor environments. Hence, we
504 conclude that tracer gas can only be adopted to simulate the dispersion of fine droplets
505 (e.g., 0.1-0.7 μm) with little deposition in coach buses.

506 ***4.3. Impacts of ventilation rates on droplet dispersion and infection risk***

507 van Doremalen et al. [6] have found that the SARS-CoV-2 virus can remain
508 infectious in aerosols for hours and up to days on surfaces, leading to probable
509 transmission. Among the three main transmission routes, the aerosol inhalation route is
510 predominant and can occur over a long distance when the ventilation is insufficient [64,
511 70]. Therefore, this study aims to investigate the mechanism of factors affecting the
512 aerosol inhalation transmission and infection risk in a crowded coach bus.

513 Enhancing the indoor ventilation rates can promote dilution and removal of
514 pathogen-laden expiratory droplets or droplet nuclei, and hence reduce the infection
515 risk [10, 67, 71]. Our study also confirms that the infection risk is closely related to
516 ventilation rates. When the ventilation rate is small, droplets can only disperse in the
517 bus rear and middle. Larger ventilation airflow drives droplets to disperse more widely
518 in the bus, but the infection risk is relatively low in the bus front (lower than 0.1% when
519 $ACH = 5.66 \text{ h}^{-1}$ for 5 μm droplets). While for tracer gas, the inhalation infection risk can

520 be reduced by an order of magnitude as ACH increases from 0.62 h^{-1} to 5.66 h^{-1} . Thus,
521 for the large range of initial diameters of respiratory droplets, the infection risk
522 decreases with the increasing ventilation rates.

523 The World Health Organization [72] has indicated that the long-range aerosol
524 inhalation transmission of COVID-19 is opportunistic in specific settings, particularly
525 in crowded and inadequately ventilated indoor environments. Li et al. [10] revealed the
526 long-range aerosol inhalation transmission in an insufficient ventilation restaurant and
527 the longest transmission distance is 4.6 m. In this outbreak, the coach bus was supplied
528 at a time-average ventilation rate of 1.72 L/s per person [11] far lower than the
529 ASHRAE Standard (2019) [73], leading to long-range aerosol inhalation transmission
530 with a longest distance of 9.46 m between the index patient and the infected passenger
531 (1D). Both simulation results and actual outbreak confirm the important role of
532 ventilation on aerosol inhalation transmission and infection risk.

533 ***4.4. Infection risk in realistic bus outbreak***

534 Another merit of this study lies in that we utilized the real outbreak data to back-
535 calculate the infection risk of each passenger according to the bus speeds and the
536 corresponding exposure time in this COVID-19 outbreak inside the coach bus. Based
537 on the numerical calculation results, we explained the following three characteristics
538 for the spatial distribution of infected passengers in this realistic epidemic: (1) more
539 infected passengers in the middle and rear of the cabin (six in Row 5-13) than in the
540 front (only one in Row 1-4); (2) more infected passengers on the index patient side (six
541 in Column C-D) than on the opposite side (only one in Column A-B).

542 The trajectory of droplets is determined by the airflow pattern, gravity force, and
543 the process of evaporation in terms of their diameter. $50 \mu\text{m}$ droplets can transmit a

544 short distance and then gradually deposit due to the gravity force, so only part of them
545 can be inhaled by passengers in the rear and middle, which leads to short-range aerosol
546 inhalation transmission [7]. Meanwhile, smaller droplets ($\leq 5 \mu\text{m}$) can continue
547 spreading to the bus front, leading to both short and long-range aerosol inhalation
548 transmissions. Thus, the infection risk is higher near the index patient and decreases
549 with distance, namely, more passengers in the middle and rear were infected than those
550 in the front.

551 Higher infection risks for both tracer gas and droplets are found on the index
552 patient's side (Column C and D). The reason may lie in the cold "gravity current" [74]
553 falling to the cabin floor and spreading throughout the entire cabin, established by the
554 skylight inlet above the aisle near the index patient. The cold "gravity current" then rose
555 with the body thermal plume of each passenger and finally exhausted at the bus front
556 skylight outlet. The blockage of the floor-level "gravity current" by the toilet in the
557 lower deck of the cabin made contaminated air spread slightly more to the index patient
558 side than to the opposite side, which brought about a higher infection risk on the index
559 patient side.

560 It can be found that there are some deviations between the realistic location of the
561 infected person and the calculated location of passengers at high infection risk. The
562 reason may lie in the following aspects. Firstly, we have calculated the infection risk of
563 aerosol inhalation transmission for droplets with some representative diameters (tracer
564 gas, $5 \mu\text{m}$, $50 \mu\text{m}$, and $100 \mu\text{m}$). However, the PLD is in the large range of diameters
565 ($0.1 - 100 \mu\text{m}$) which may highly affect the infection risk. Thus, it needs further study
566 on the infection risk distribution of droplets in large range of diameters. Secondly, there
567 are many other factors that may affect passengers being infected, such as other

568 transmission routes (e.g., direct-contact/indirect-contact transmission [75]), immunity
569 of passengers, the activity status of passengers in the bus (wear a mask or not, speak or
570 not, etc). However, our study quantified the impact of natural ventilation on the
571 infection risk of tracer gas and droplets and provided a basis for the prevention and
572 control of respiratory infectious diseases in coach buses.

573

574 *4.5. Limitations and future research*

575 There are several limitations of the present research that should be acknowledged.
576 Different respiratory activities, including breathing, speaking, coughing, sneezing, etc,
577 can affect the generation and dispersion of droplets [26, 58, 76]. We only considered
578 the index patient's breathing activity, because the epidemiological survey suggests that
579 the index patient did not cough or talk to anyone during the whole trip. In the future,
580 we will further consider more respiratory activities and more influencing parameters
581 (e.g., natural ventilation modes by opening windows, source location, ambient
582 temperature, different total heat flux for occupant etc). Meanwhile, it deserves further
583 investigation on how the droplet final fates change with various ventilation rates and
584 initial diameters under the combined effect of ambient airflow, gravity and body thermal
585 plumes. Due to the positive pressure at the bus rear and the negative pressure at the bus
586 front, opening the windows at the bus rear is beneficial to increase the ventilation rates,
587 but the specific method needs further evaluation. Additionally, during the epidemic of
588 infectious disease, public vehicles are required to be less than half occupancy in order
589 to reduce the infection risk, which has not only caused great economic losses to the
590 transportation operation companies, but also caused inconvenience to people's travel.
591 Therefore, it is worth further investigating the infection risk under different seat

592 arrangements to give a more specific suggestion for arranging the occupancy in
593 different coach buses.

594

595 **5. Conclusions**

596 Based on experiments of one-infecting-seven COVID-19 outbreak with an index
597 patient at bus rear, this paper performed CFD simulations to explore the PLD dispersion
598 and infection risk in a crowded coach bus, which is important but still scarce. The
599 integrated effects of initial droplet diameters, natural air change rates per hour and
600 relative humidity are considered.

601 Some meaningful conclusions can be stated:

602 (1) In this bus epidemic, inadequate ventilation, crowded passengers and long
603 exposure time (200 min) are the main reasons for the large number of infected
604 passengers (i.e., seven) with a longest infected distance of 9.46 m.

605 (2) The pressure difference between the bus rear and front makes the air enter the
606 bus from the rear ceiling-level skylight (inlet), and leave through the bus front
607 ceiling-level skylight (outlet), carrying droplets/tracer gas disperse from the
608 rear to the front. Higher bus speed leads to more ventilation rates.

609 (3) Tracer gas can only be adopted to simulate fine droplet (e.g., 0.1-0.7 μm)
610 dispersion in coach buses. The gaseous inhalation transmission can occur in
611 the entire cabin, and its infection risk is greatly reduced with the increasing
612 ventilation rates. When *ACH* increases from 0.62 h^{-1} to 2.27 h^{-1} and 5.66 h^{-1} ,
613 *TIF* of tracer gas for each passenger decreases from 11.10-15.29% to 3.20-
614 13.08% and 1.27-3.09%.

615 (4) Over 99.5%/97.0% of large droplets (i.e., 100 μ m/50 μ m) deposit locally due to
616 gravity. Thus, the *TIF* of 100 μ m/50 μ m droplets is almost independent of *ACH*,
617 with a peak *TIF* (~3.1%) near the index patient. Because gravity is less
618 significant for 5 μ m droplets which can spread more widely with the
619 ventilation airflow from bus rear to front and disperse even further with the
620 increasing ventilation.

621 (5) Unlike ordinary rooms, most droplets will deposit on objects when spread in
622 the long-and-narrow bus, but tracer gas will not deposit. therefore, the
623 infection risk of tracer gas is obviously higher than that of 5-100 μ m droplets.

624 (6) Relative humidity (*RH*=35% and 95%) affects the droplet evaporation process,
625 but insignificantly influences the dispersion and infection risk.

626 For coach buses and other indoor environments, fresh air should be sufficiently
627 supplied for the occupants. When the occupancy rate of vehicles is high, it is
628 recommended to open windows or ceiling-level skylight at the vehicle rear to attain
629 more fresh air into the bus and better natural ventilation. Even for cold winter or hot
630 summer, we should find a balance between energy consumption and human health, i.e.,
631 to ensure thermal comfort by air conditioners or heating devices meanwhile provide
632 sufficient external fresh air by opening ceiling-level skylight or small-area windows to
633 reduce the infection risk in the vehicle.

634

635 **Acknowledgements**

636 This work was supported by the National Natural Science Foundation of China
637 (grant numbers 41875015, 42005069, and 42175180); the Special Fund (International
638 Cooperation) Project for Science and Technology Innovation Strategy of Guangdong

639 Province (China, grant number 2019A050510021); Research and development projects
640 in key areas of Guangdong Province (code 212020012620600004). The support from
641 UK GCRF Rapid Response Grant on ‘Transmission of SARS-CoV-2 virus in crowded
642 indoor environment’, the Opening Fund of State Key Laboratory of Green Building in
643 Western China (No. LSKF202106), the Innovation Group Project of the Southern
644 Marine Science and Engineering Guangdong Laboratory (Zhuhai) (No. 311020001),
645 are also gratefully acknowledged. The supports by National Supercomputer Center in
646 Guangzhou, P.R. China are also gratefully acknowledged.

647

648 **References**

- 649 [1] World Health Organization (WHO), Modes of transmission of virus causing
650 COVID-19: implications for IPC precaution recommendations: scientific brief,
651 (Accessed 29 March 2020). <https://apps.who.int/iris/handle/10665/331616>
- 652 [2] World Health Organization (WHO), WHO Coronavirus (Covid-19) Dashboard,
653 (2021). <https://covid19.who.int/>
- 654 [3] S. Asadi, N. Bouvier, A. Wexler, W. Ristenpart, The coronavirus pandemic and
655 aerosols: Does COVID-19 transmit via expiratory particles, *Aerosol Sci. Technol.*
656 *54*(6) (2020) 635-638. <https://doi.org/10.1080/02786826.2020.1749229>
- 657 [4] Y. Drossinos, N. Stilianakis, What aerosol physics tells us about airborne
658 pathogen transmission, *Aerosol Sci. Technol.* *54*(6) (2020) 639-643. <https://doi.org/10.1080/02786826.2020.1751055>
- 660 [5] J. Kutter, M. Spronken, P. Fraaij, R. Fouchier, S. Herfst, Transmission routes of
661 respiratory viruses among humans, *Curr. Opin. Virol.* *28* (2018) 142-151. <https://doi.org/10.1016/j.coviro.2018.01.001>
- 663 [6] N. van Doremalen, T. Bushmaker, D. Morris, M. Holbrook, V. Munster, Aerosol
664 and surface stability of SARS-CoV-2 as compared with SARS-CoV-1, *N. Engl. J.*
665 *Med.* *382*(16) (2020) 1564-1567. <https://doi.org/10.1056/NEJMc2004973>
- 666 [7] Y. Li, Basic routes of transmission of respiratory pathogens—A new proposal for
667 transmission categorization based on respiratory spray, inhalation, and touch, *Indoor*
668 *Air* *31*(1) (2021) 3-6. <https://doi.org/10.1111/ina.12786>

- 669 [8] L. Marr, J. Tang, A Paradigm Shift to Align Transmission Routes With
670 Mechanisms, *Clin. Infect. Dis.* 73(10) (2021) 1747-1749. [https://doi.org/10.1093/cid/
671 ciab722](https://doi.org/10.1093/cid/ciab722)
- 672 [9] J. Hang, Y. Li, R. Jin, The influence of human walking on the flow and airborne
673 transmission in a six-bed isolation room: tracer gas simulation, *Build. Environ.* 77
674 (2014) 119-134. <https://doi.org/10.1016/j.buildenv.2014.03.029>
- 675 [10] Y. Li, H. Qian, J. Hang, X. Chen, P. Cheng, H. Ling, S. Wang, P. Liang, J. Li, S.
676 Xiao, Probable airborne transmission of SARS-CoV-2 in a poorly ventilated
677 restaurant, *Build. Environ.* 196 (2021) 107788. [https://doi.org/10.1016/j.buildenv.
678 2021.107788](https://doi.org/10.1016/j.buildenv.2021.107788)
- 679 [11] C. Ou, S. Hu, K. Luo, H. Yang, J. Hang, P. Cheng, Z. Hai, S. Xiao, H. Qian, S.
680 Xiao, Insufficient ventilation led to a probable long-range airborne transmission of
681 SARS-CoV-2 on two buses, *Build. Environ.* 207 (2022) 108414. [https://doi.org/10.
682 1016/j.buildenv.2021.108414](https://doi.org/10.1016/j.buildenv.2021.108414)
- 683 [12] M. Kang, J. Wei, J. Yuan, J. Guo, Y. Zhang, J. Hang, Y. Qu, H. Qian, Y.
684 Zhuang, X. Chen, Probable evidence of fecal aerosol transmission of SARS-CoV-2 in
685 a high-rise building, *Ann. Intern. Med.* 173(12) (2020) 974-980. [https://doi.org/10.
686 7326/M20-0928](https://doi.org/10.7326/M20-0928)
- 687 [13] X. Liu, J. Niu, K. Kwok, Analysis of concentration fluctuations in gas dispersion
688 around high-rise building for different incident wind directions, *J. Hazard. Mater.*
689 192(3) (2011) 1623-1632. <https://doi.org/10.1016/j.jhazmat.2011.06.090>
- 690 [14] X. Liu, J. Niu, K. Kwok, J. Wang, B. Li, Local characteristics of cross-unit
691 contamination around high-rise building due to wind effect: mean concentration and
692 infection risk assessment, *J. Hazard. Mater.* 192(1) (2011) 160-167. [https://doi.org/10.
693 1016/j.jhazmat.2011.04.106](https://doi.org/10.1016/j.jhazmat.2011.04.106)
- 694 [15] Q. Wang, Y. Li, D. Lung, P. Chan, C. Dung, W. Jia, T. Miao, J. Huang, W.
695 Chen, Z. Wang, Aerosol transmission of SARS-CoV-2 due to the chimney effect in
696 two high-rise housing drainage stacks, *J. Hazard. Mater.* 421 (2022) 126799. [https://
697 doi.org/10.1016/j.jhazmat.2021.126799](https://doi.org/10.1016/j.jhazmat.2021.126799)
- 698 [16] I. Yu, Y. Li, T. Wong, W. Tam, A. Chan, J. Lee, D. Leung, T. Ho, Evidence of
699 airborne transmission of the severe acute respiratory syndrome virus, *N. Engl. J. Med.*
700 350(17) (2004) 1731-1739. <https://doi.org/10.1056/nejmoa032867>
- 701 [17] L. Liu, Y. Li, P. Nielsen, J. Wei, R. Jensen, Short-range airborne transmission of
702 expiratory droplets between two people, *Indoor Air* 27(2) (2017) 452-462. [https://doi.
703 org/10.1111/ina.12314](https://doi.org/10.1111/ina.12314)

- 704 [18] L. Liu, J. Wei, Y. Li, A. Ooi, Evaporation and dispersion of respiratory droplets
705 from coughing, *Indoor Air* 27(1) (2017) 179-190. <https://doi.org/10.1111/ina.12297>
- 706 [19] F. Liu, Z. Luo, Y. Li, X. Zheng, C. Zhang, H. Qian, Revisiting physical
707 distancing threshold in indoor environment using infection-risk-based modeling,
708 *Environ. Int.* 153 (2021) 106542. <https://doi.org/10.1016/j.envint.2021.106542>
- 709 [20] N. Zhang, X. Chen, W. Jia, T. Jin, S. Xiao, W. Chen, J. Hang, C. Ou, H. Lei, H.
710 Qian, B. Su, J. Li, D. Liu, Evidence for lack of transmission by close contact and
711 surface touch in a restaurant outbreak of COVID-19, *J. Infect.* 83 (2021) 207-216.
712 <https://doi.org/10.1016/j.jinf.2021.05.030>
- 713 [21] J. Hang, Y. Li, W. Ching, J. Wei, R. Jin, L. Liu, X. Xie, Potential airborne
714 transmission between two isolation cubicles through a shared anteroom, *Build.*
715 *Environ.* 89 (2015) 264-278. <https://doi.org/10.1016/j.buildenv.2015.03.004>
- 716 [22] H. Qian, Y. Li, P. Nielsen, C. Hyldgaard, T. Wong, A. Chwang, Dispersion of
717 exhaled droplet nuclei in a two-bed hospital ward with three different ventilation
718 systems, *Indoor Air* 16(2) (2006) 111-128. <https://doi.org/10.1111/j.1600-0668.2005.00407.x>
- 720 [23] I. Bogoch, A. Watts, A. Thomas-Bachli, C. Huber, K. Khan, Pneumonia of
721 unknown aetiology in Wuhan, China: potential for international spread via
722 commercial air travel, *J. Travel Med.* 27(2) (2020) 1-3. [https://doi.org/10.1093/](https://doi.org/10.1093/jtm/taaa008)
723 [jtm/taaa008](https://doi.org/10.1093/jtm/taaa008)
- 724 [24] J. Gupta, C. Lin, Q. Chen, Transport of expiratory droplets in an aircraft cabin,
725 *Indoor Air* 21(1) (2011) 3-11. <https://doi.org/10.1111/j.1600-0668.2010.00676.x>
- 726 [25] L. Oztig, O. Askin, Human mobility and coronavirus disease 2019 (COVID-19):
727 a negative binomial regression analysis, *Public Health* 185 (2020) 364-367. [https://](https://doi.org/10.1016/j.puhe.2020.07.002)
728 doi.org/10.1016/j.puhe.2020.07.002
- 729 [26] L. Zhang, Y. Li, Dispersion of coughed droplets in a fully-occupied high-speed
730 rail cabin, *Build. Environ.* 47 (2012) 58-66. [https://doi.org/10.1016/j.buildenv.2011.](https://doi.org/10.1016/j.buildenv.2011.03.015)
731 [03.015](https://doi.org/10.1016/j.buildenv.2011.03.015)
- 732 [27] S. Zhao, Z. Zhuang, J. Ran, J. Lin, G. Yang, L. Yang, D. He, The association
733 between domestic train transportation and novel coronavirus (2019-nCoV) outbreak in
734 China from 2019 to 2020: a data-driven correlational report, *Travel Med. Infect. Dis.*
735 33 (2020) 101568. <https://doi.org/10.1016/j.tmaid.2020.101568>
- 736 [28] X. Yang, C. Ou, H. Yang, L. Liu, T. Song, M. Kang, H. Lin, J. Hang,
737 Transmission of pathogen-laden expiratory droplets in a coach bus, *J. Hazard. Mater.*
738 397 (2020) 122609. <https://doi.org/10.1016/j.jhazmat.2020.122609>

- 739 [29] R. Zheng, Y. Xu, W. Wang, G. Ning, Y. Bi, Spatial transmission of COVID-19
 740 via public and private transportation in China, *Travel Med. Infect. Dis.* 34 (2020)
 741 101626. <https://doi.org/10.1016/j.tmaid.2020.101626>
- 742 [30] C. Chao, P. Man, L. Morawska, G. Johnson, D. Katoshevski, Characterization of
 743 expiration air jets and droplet size distributions immediately at the mouth opening, *J.*
 744 *Aerosol Sci.* 40(2) (2009) 122-133. <https://doi.org/10.1016/j.jaerosci.2008.10.003>
- 745 [31] L. Morawska, G. Johnson, Z. Ristovski, M. Hargreaves, K. Mengersen, S.
 746 Corbett, C. Chao, Y. Li, D. Katoshevski, Size distribution and sites of origin of
 747 droplets expelled from the human respiratory tract during expiratory activities, *J.*
 748 *Aerosol Sci.* 40(3) (2009) 256-269. <https://doi.org/10.1016/j.jaerosci.2008.11.002>
- 749 [32] J. Wei, Y. Li, Enhanced spread of expiratory droplets by turbulence in a cough
 750 jet, *Build. Environ.* 93 (2015) 86-96. <https://doi.org/10.1016/j.buildenv.2015.06.018>
- 751 [33] X. Xie, Y. Li, A. Chwang, P. Ho, W. Seto, How far droplets can move in indoor
 752 environments-revisiting the Wells evaporation-falling curve, *Indoor Air* 17(3) (2007)
 753 211-225. <https://doi.org/10.1111/j.1600-0668.2007.00469.x>
- 754 [34] Y. Tung, Y. Shih, S. Hu, Numerical study on the dispersion of airborne
 755 contaminants from an isolation room in the case of door opening, *Appl. Therm. Eng.*
 756 29 (2009) 1544-1551. <https://doi.org/10.1016/j.applthermaleng.2008.07.009>
- 757 [35] J. Villafruela, I. Olmedo, J. José, Influence of human breathing modes on
 758 airborne cross infection risk, *Build. Environ.* 106 (2016) 340-351. <https://doi.org/10.1016/j.buildenv.2016.07.005>
- 760 [36] Y. Yin, W. Xu, J. Gupta, A. Guity, P. Marmion, A. Manning, B. Gulick, X.
 761 Zhang, Q. Chen, Experimental study on displacement and mixing ventilation systems
 762 for a patient ward, *HVAC R. Res.* 15(6) (2009) 1175-1191. <https://doi.org/10.1080/10789669.2009.10390885>
- 764 [37] R. Cermak, A. Melikov, Protection of occupants from exhaled infectious agents
 765 and floor material emissions in rooms with personalized and underfloor ventilation,
 766 *HVAC R. Res.* 13(1) (2007) 23-38. <https://doi.org/10.1080/10789669.2007.10390942>
- 767 [38] J. Redrow, S. Mao, I. Celik, J. Posada, Z. Feng, Modeling the evaporation and
 768 dispersion of airborne sputum droplets expelled from a human cough, *Build. Environ.*
 769 46(10) (2011) 2042-2051. <https://doi.org/10.1016/j.buildenv.2011.04.011>
- 770 [39] V. Yakhot, S. Orszag, Renormalization group analysis of turbulence. I. Basic
 771 theory, *J. Sci. Comput.* 1(1) (1986) 3-51.
- 772 [40] T. Zhang, Q. Chen, Identification of contaminant sources in enclosed spaces by a
 773 single sensor, *Indoor Air* 17(6) (2007) 439-449. <https://doi.org/10.1111/j.1600-0668.2007.00489.x>
- 774

- 775 [41] Z. Zhang, W. Zhang, Z. Zhai, Q. Chen, Evaluation of various turbulence models
776 in predicting airflow and turbulence in enclosed environments by CFD: Part 2—
777 Comparison with experimental data from literature, HVAC R. Res. 13(6) (2007) 871-
778 886. <https://doi.org/10.1080/10789669.2007.10391460>
- 779 [42] Z. Zhang, X. Chen, S. Mazumdar, T. Zhang, Q. Chen, Experimental and
780 numerical investigation of airflow and contaminant transport in an airliner cabin
781 mockup, Build. Environ. 44(1) (2009) 85-94. <https://doi.org/10.1016/j.buildenv.2008.01.012>
782
- 783 [43] Z. Zhang, Q. Chen, Comparison of the Eulerian and Lagrangian methods for
784 predicting particle transport in enclosed spaces, Atmos. Environ. 41(25) (2007) 5236-
785 5248. <https://doi.org/10.1016/j.atmosenv.2006.05.086>
- 786 [44] H. Qian, Y. Li, Removal of exhaled particles by ventilation and deposition in a
787 multibed airborne infection isolation room, Indoor air 20(4) (2010) 284-297. <https://doi.org/10.1111/j.1600-0668.2010.00653.x>
788
- 789 [45] R. Clift, J. Grace, M. Weber, Bubbles, drops, and particles, Academic Press
790 (1978). <https://doi.org/10.1080/07373939308916817>
- 791 [46] W. Hinds, Aerosol technology: properties, behavior, and measurement of
792 airborne particles, John Wiley & Sons (1999).
- 793 [47] J. Potter, L. Matthews, J. Lemm, S. Spector, Human pulmonary secretions in
794 health and disease, Ann. N. Y. Acad. Sci. 106(2) (1963) 692-697. <https://doi.org/10.1111/j.1749-6632.1963.tb16677.x>
795
- 796 [48] W. Ranz, Marshall, W., Evaporation from drops, Part II, Chem. Eng. Prog. 48(4)
797 (1952) 7.
- 798 [49] P. Zhao, Y. Li, Correlation between the normal position of a particle on a rough
799 surface and the van der Waals force, Colloids Surf. A Physicochem. Eng. Asp. 585
800 (2020) 124096. <https://doi.org/10.1016/j.colsurfa.2019.124096>
- 801 [50] A. Magar, M. Joshi, P. Rajagopal, A. Khan, M. Rao, B. Saprana, CFD simulation
802 of the airborne transmission of covid-19 vectors emitted during respiratory
803 mechanisms : Revisiting the concept of safe distance. ACS Omega 6 (2021) 16876–
804 16889. <https://doi.org/10.1021/acsomega.1c01489>
- 805 [51] X. Shao, X. Li, COVID-19 transmission in the first presidential debate in 2020.
806 Phys. Fluids 32 (2020) 1–9. <https://doi.org/10.1063/5.0032847>
- 807 [52] H. Qian, Y. Li, P. Nielsen, X. Huang, Spatial distribution of infection risk of
808 SARS transmission in a hospital ward. Build. Environ. 44 (2009) 1651–1658. <https://doi.org/10.1016/j.buildenv.2008.11.002>
809

810 [53] G. Buonanno, L. Stabile, L. Morawska, Estimation of airborne viral emission:
811 Quanta emission rate of SARS-CoV-2 for infection risk assessment. *Environ. Int.* 141
812 (2020) 105794. <https://doi.org/10.1016/j.envint.2020.105794>

813 [54] E. Riley, G. Murphy, R. Riley, Airborne spread of measles in a suburban
814 elementary school, *Am. J. Epidemiol.* 107 (1978) 421-432. [https://doi.org/10.1093/
815 oxfordjournals.aje.a112560](https://doi.org/10.1093/oxfordjournals.aje.a112560)

816 [55] S. Zhang, Z. Lin, Dilution-based evaluation of airborne infection risk-Thorough
817 expansion of Wells-Riley model, *Build. Environ.* 194 (2021) 107674. [https://doi.org/
818 10.1016/j.buildenv.2021.107674](https://doi.org/10.1016/j.buildenv.2021.107674)

819 [56] H. Dai, B. Zhao, Association of the infection probability of COVID-19 with
820 ventilation rates in confined spaces, *Build. Simul.* 13 (2020) 1321-1327. [https://doi.
821 org/10.1007/s12273-020-0703-5](https://doi.org/10.1007/s12273-020-0703-5)

822 [57] H. Yang, T. Chen, Y. Lin, R. Buccolieri, M. Mattsson, M. Zhang, J. Hang, Q.
823 Wang, Integrated impacts of tree planting and street aspect ratios on CO dispersion
824 and personal exposure in full-scale street canyons. *Build. Environ.* 169 (2020)
825 106529. <https://doi.org/10.1016/j.buildenv.2019.106529>

826 [58] M. Mesgarpour, J. Abad, R. Alizadeh, S. Wongwises, M. Doranehgard, S.
827 Ghaderi, N. Karimi, Prediction of the spread of Corona-virus carrying droplets in a
828 bus-A computational based artificial intelligence approach, *J. Hazard. Mater.* 413
829 (2021) 125358. <https://doi.org/10.1016/j.jhazmat.2021.125358>

830 [59] W. Duan, D. Mei, J. Li, Z. Liu, M. Ja, S. Hou, Spatial distribution of exhalation
831 droplets in the bus in different seasons, *Aerosol Air Qual. Res.* 21 (2021) 200478-
832 200478. <https://doi.org/10.4209/aaqr.200478>

833 [60] S. Sun, J. Li, J. Han, How human thermal plume influences near-human transport
834 of respiratory droplets and airborne particles: a review, *Environ. Chem. Lett.* 19
835 (2021) 1971-1982. <https://doi.org/10.1007/s10311-020-01178-4>

836 [61] C. Yang, X. Yang, B. Zhao, The ventilation needed to control thermal plume and
837 particle dispersion from manikins in a unidirectional ventilated protective isolation
838 room, *Build. Simul.* 8(5) (2015) 551-565. <https://doi.org/10.1007/s12273-014-0227-6>

839 [62] C. Chen, B. Zhao, Some questions on dispersion of human exhaled droplets in
840 ventilation room: answers from numerical investigation, *Indoor Air* 20(2) (2010) 95-
841 111. <https://doi.org/10.1111/j.1600-0668.2009.00626.x>

842 [63] A. Tsuda, F. Henry, J. Butler, Particle transport and deposition: basic physics of
843 particle kinetics, *Compr. Physiol.* 3(4) (2013) 1437-1471. [https://doi.org/10.1002/
844 cphy.c100085](https://doi.org/10.1002/cphy.c100085)

- 845 [64] W. Chen, N. Zhang, J. Wei, H. Yen, Y. Li, Short-range airborne route dominates
846 exposure of respiratory infection during close contact, *Build. Environ.* 176 (2020)
847 106859. <https://doi.org/10.1016/j.buildenv.2020.106859>
- 848 [65] Y. Ji, H. Qian, J. Ye, X. Zheng, The impact of ambient humidity on the
849 evaporation and dispersion of exhaled breathing droplets: A numerical investigation,
850 *J. Aerosol Sci.* 115 (2018) 164-172. <https://doi.org/10.1016/j.jaerosci.2017.10.009>
- 851 [66] S. Zhu, S. Kato, J. Yang, Study on transport characteristics of saliva droplets
852 produced by coughing in a calm indoor environment, *Build. Environ.* 41(12) (2006)
853 1691-1702. <https://doi.org/10.1016/j.buildenv.2005.06.024>
- 854 [67] Q. He, J. Niu, N. Gao, T. Zhu, J. Wu, CFD study of exhaled droplet transmission
855 between occupants under different ventilation strategies in a typical office room,
856 *Build. Environ.* 46(2) (2011) 397-408. <https://doi.org/10.1016/j.buildenv.2010.08.003>
- 857 [68] Z. Zhao, C. Xi, S. Mazumdar, T. Zhang, Q. Chen, Experimental and numerical
858 investigation of airflow and contaminant transport in an airliner cabin mockup, *Build.*
859 *Environ.* 44(1) (2009) 85-94. <https://doi.org/10.1016/j.buildenv.2008.01.012>
- 860 [69] A. Lai, W. Nazaroff, Modeling indoor particle deposition from turbulent flow
861 onto smooth surfaces, *J. Aerosol Sci.* 31(4) (2000) 463-476. [https://doi.org/10.1016/
862 S0021-8502\(99\)00536-4](https://doi.org/10.1016/S0021-8502(99)00536-4)
- 863 [70] W. Chen, H. Qian, N. Zhang, F. Liu, L. Liu, Y. Li, Extended short-range airborne
864 transmission of respiratory infections, *J. Hazard. Mater.* 422 (2022) 126837.
865 <https://doi.org/10.1016/j.jhazmat.2021.126837>
- 866 [71] M. Mirzaie, E. Lakzian, A. Khan, M. Warkiani, O. Mahian, G. Ahmadi, COVID-
867 19 spread in a classroom equipped with partition—A CFD approach, *J. Hazard. Mater.*
868 420 (2021) 126587. <https://doi.org/10.1016/j.jhazmat.2021.126587>
- 869 [72] World Health Organization (WHO), Coronavirus disease (COVID-19): How is it
870 transmitted, (Accessed 13 December 2020). [https://www.who.int/news-room/q-a-
871 detail/coronavirus-disease-covid-19-how-is-it-transmitted](https://www.who.int/news-room/q-a-detail/coronavirus-disease-covid-19-how-is-it-transmitted)
- 872 [73] American Society of Heating, Refrigerating and Air-Conditioning Engineers
873 (ASHRAE) Ventilation for acceptable indoor air quality, ASHRAE Standard, Atlanta,
874 USA (2019).
- 875 [74] D. Etheridge, M. Sandberg, Building ventilation: theory and measurement, John
876 Wiley & Sons Chichester, UK (1996).
- 877 [75] P. Cheng, K. Luo, S. Xiao, H. Yang, J. Hang, C. Ou, B. Cowling, H. Yen, D. Sc,
878 S. Hu, Y. Li, Predominant airborne transmission and insignificant fomite transmission
879 of SARS-CoV-2 in a two-bus COVID-19 outbreak originating from the same pre-
880 symptomatic index case. *J. Hazard. Mater.* 425 (2022) 128051. [https://doi.org/
881 10.1016/j.jhazmat.2021.128051](https://doi.org/10.1016/j.jhazmat.2021.128051)

882 [76] J. Gupta, C. Lin, Q. Chen, Inhalation of expiratory droplets in aircraft cabins,
883 Indoor Air 21(4) (2011) 341-350. <https://doi.org/10.1111/j.1600-0668.2011.00709.x>
884
885